Institut de recherche
pour le développement

Research internship report

Diurnal rainfall cycle over New Caledonia in warm season (November-April) : influence of Madden-Julian oscillation and weather regimes

Damien Specq

Program	: WAPE Master
Program supervisor	: Claude Basdevant
Supervisors	: Christophe Eugène Menkes, Jérôme Lefèvre
Co-supervisor	: Gilles Bellon
Dates	: April, 11th, 2016 - August, 12th, 2016
Laboratory	: IRD/LOCEAN
Adress	: IRD, 101 Promenade Roger Laroque BP A5 98848 NOUMEA CEDEX NEW CALEDONIA

Remerciements

Ces remerciements apparaissent dans le désordre le plus total car tout le monde devrait être en premier :

Christophe, sans qui il n'y aurait eu ni stage, ni Nouvelle-Calédonie. Un immense merci de m'avoir donné la possibilité d'essayer de comprendre la pluie et le beau temps à l'autre bout du monde. Un grand merci également pour avoir supporté mes questions incessantes et pour avoir su clarifier les directions à prendre quand les voies de la science se montraient confuses et impénétrables.

Jérôme, pour avoir aussi supporté mes nombreuses questions, pour ta disponibilité sans faille et ton aide cruciale sur la physique de l'atmosphère comme sur les mystères de l'informatique, pour les nombreuses références et les précieuses données de simulation.

Gilles, pour les deux semaines d'invitation à l'université d'Auckland, étape déterminante dans l'avancée de ce stage et formidable occasion d'avoir un petit aperçu de la Nouvelle-Zélande et de la culture Kiwi. Merci aussi pour les précieux conseils pour l'avenir, et bien sûr merci pour avoir géré les aspects financiers du stage. Un grand merci également à Nicolas pour les conseils avisés pour améliorer cette étude dans le cadre du projet PLUVAR lors de notre entretien à Auckland.

Alexandre, pour les données pluviométriques, les visites et les rencontres à Météo France Nouvelle-Calédonie.

Cyril, pour ne pas m'avoir expulsé de ton bureau malgré mes dernières questions informatiques (parfois stupides), pour ta bonne humeur, ton sens de l'humour et pour ton cycle saisonnier des pluies...

Toute la bande des lofteurs, stagiaires et doctorants de l'IRD, pour l'accueil, la chaleur, la bienveillance, les soirées, les sorties, les week-ends, les jeux et l'ambiance conviviale grâce à laquelle ce séjour à Nouméa restera un souvenir inoubiable...

Abstract

Rainfall diurnal variability in the Mainland of New Caledonia (SW Pacific) is investigated using 24 years of hourly rain gauge warm season (November-April) data at 29 meteorological stations. We link this variability to the Madden-Julian Oscillation (MJO) via the determination of four warm season synoptic circulation regimes over the archipelago during the same period with the NOAA/NCDC Blended Sea Winds data. A statistical analysis completed by a study of subtropical circulation anomalies in the Pacific basin associated to the MJO enables to find a relationship between MJO phases and synoptic circulation regimes for which the impact on the diurnal cycle of New Caledonian precipitation is analyzed. Spatial clustering of rain gauge stations enables to determine four main zones that exhibit distinct behavior in the changes of their diurnal cycle associated with weather regimes. Eventually, the mechanisms for this relationship between synoptic circulation and rainfall diurnal variability are investigated with a 5-year 4-km resolution simulation output obtained with the Weather Research and Forecasting (WRF) model, version 2.2. There is strong evidence for an average standard diurnal cycle over the Mainland with a precipitation peak in the afternoon aroud 03 :00 PM, that is associated to wind and moisture convergence on the mountain range. The impact of this diurnal cycle extends to the West coast of the Mainland while the East coast is prone to an altogether different rainfall variability in general, with higher sustained precipitation throughout the day. Yet, this divergent East coast behavior can be modified and correlated to the diurnal cycle in the rest of the island in the case of a particular, southerly-oriented synoptic circulation that interacts with the strong West coast sea breeze. The impact of weather regimes and, indirectly, of the MJO, on the diurnal cycle of precipitation is therefore not only a matter of average precipitation (some regimes are rainier than the others) but also of orientation of the dominant winds.

Keywords : Island precipitation, diurnal variability, Madden-Julian Oscillation, circulation weather types, spatial clustering, mesoscale model

Table of contents

Introduction

Rainfall in the tropical Pacific exhibits several distinct time scales of variability, ranging from the diurnal cycle to interannual variations with the El Niño Southern Oscillation. While the variability on time scales between seasonal and interannual is crucial to plan water availability and has been well documented, the impact of shorter-term variations remains to be studied extensively. Through the example of New Caledonia, this report aims at bringing additional information on the interaction between two modes of short-term variability for tropical island rainfall : the diurnal cycle and the Madden-Julian oscillation (MJO), which is the dominant component of intraseasonal (30-90 days) variability in the Tropics. The distribution of precipitation events at these short time scales is indeed essential for some climate impacts that must be taken into account for public policies, such as flooding, drought, erosion or even the outbreak of vectorial diseases epidemics.

A general characteristic of tropical island climate is the important diurnal cycle due to the switch from sea breeze (in the afternoon) to land breeze (at the end of the night), owing to the difference of heat capacity between the island and the ocean : the magnitude of the warming and cooling of the island with the day-night alternance is far more important than that of the ocean. The convergence of moist air over the island favors precipitation, and this can also be intensified by orographic effects in the case of mountainous islands. Therefore, tropical islands are on average more rainy than the surrounding ocean (Sobel et al., 2011; Cronin et al., 2015).

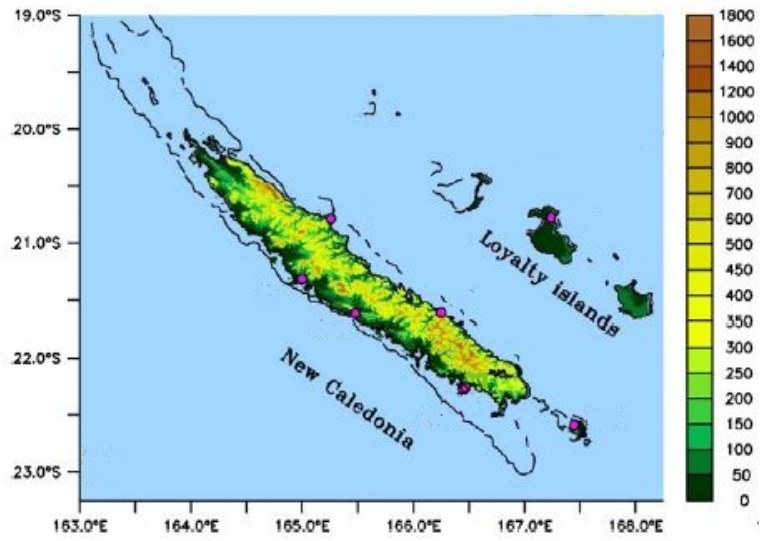

FIGURE 1 – Geography of New Caledonia : Mainland and dependences. Altitude in m. (adapted from Lefèvre et al. (2010))

New Caledonia is a group of islands in the subtropical southwest Pacific Ocean, around 20°S and 166°E. It is made up of a long main island called the Mainland or « Grande Terre », an archipelago (with three islands) called the Loyalty Islands to the east of the Mainland, the Isle of Pines to the

south and another archipelago called Belep to the north (see Figure 1). The Mainland is oriented along the northwest-southeast trade winds axis. It is approximately 400 km long and 50 km wide, with a central mountain range and it is surrounded by a shallow lagoon. The mountain range is 800 m high on average with two highest peaks located on the east coast, Mount Humboldt to the south (1618 m) and Mount Panié to the north (1628 m). The mountain slopes are steeper on the eastern shore of the Mainland, where they also stand closer to the sea. On the contrary, the Loyalty Islands, the Isle of Pines and the Belep archipelago are roughly flat and low-lying islands. Given data availability and the huge difference of size between the Mainland and the other islands of New Caledonia, this study will only focus on the diurnal cycle of precipitation over the Mainland. At this point, it must be specified that a temporal restriction is also added, since the study only focuses on New Caledonia warm seasons (November to April) because the MJO events are more frequent and stronger during this period.

After a review of the work previously done on the diurnal cycle and the meteorological impacts of the MJO in other regions of the world (such as the Maritime Continent) and in New Caledonia, the first step of our analysis will be to look for the general features of rainfall over the Mainland and the direct impacts of the different phases of the Madden-Julian oscillation on it, based on observational datasets and model data. Then, we will design a classification of synoptic scale wind circulation regimes so as to gain a better physical understanding of how the MJO phases can alter the diurnal cycle. These synoptic weather types will be linked to MJO phases through statistics and the dynamics of large scale patterns. Next, the effect of synoptic circulation on the diurnal cycle will be analyzed extensively with a spatial classification of several geographical areas of the Mainland according to the dependence of their diurnal cycle on the weather regimes. This study will end on a mesoscale model analysis in order to provide a plausible explanation for the variability of the rainfall diurnal cycle with the orientation of synoptic winds.

Literature review

1.1 Madden-Julian oscillation

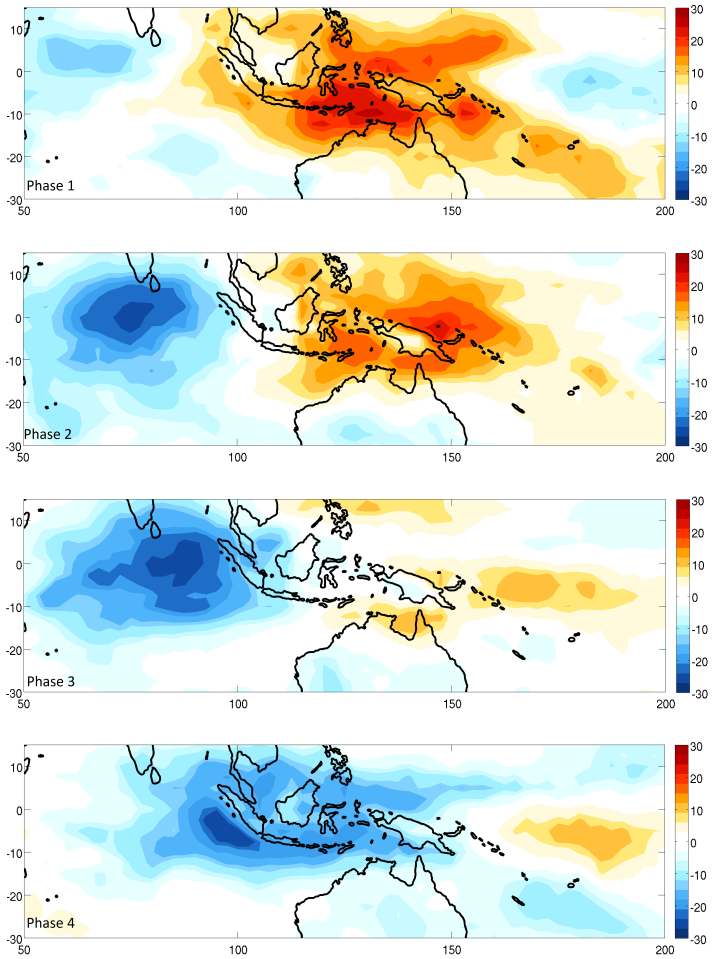

FIGURE 1.2 – Outgoing Longwave Radiation (OLR) anomalies OLR [a] in W/m^2 (as defined in Wheeler and Hendon (2004)) for MJO phases 1 to 4. Negative OLR anomalies : enhanced convection. Positive OLR anomalies : suppressed convection.

The Madden-Julian oscillation (Madden and Julian, 1971) is a propagating atmospheric process that develops in the Indian Ocean and mostly occurs in the tropical band over the Indian and Pacific basins at intraseasonal time scale with a period ranging from 30 to 90 days. It consists of a large-scale coupling between atmospheric circulation and deep convection that propagates eastward at an approximate speed of 5 m/s (Zhang, 2005). One of its most striking features is the presence of an equatorial patch of enhanced deep convection, that increases cloud cover and precipitation and can

be noted through a reduction (negative anomaly) in the Outgoing Longwave Radiation (OLR). It comes along with a similar patch of suppressed convection (positive OLR anomaly, see Figures 1.2 and 1.3), where there is less rainfall than average. This pattern with a zonal alternance between enhanced and suppressed convection moves eastward over the zones of warm sea surface temperature (SST) and modulates rainfall in the tropical band. Because of the coupling between atmospheric circulation and convection, the MJO is also associated to large-scale circulation anomalies and oscillations, as illustrated by the founding work of Madden and Julian (1971) in which the MJO was discovered as an oscillation of the zonal wind. In accordance with the theoretical model developed by Gill (1980) on tropical circulation induced by diabatic heating, Rui and Wang (1990) have noted that the intraseasonal equatorial convection anomalies are responsible for anomalous cyclonic or anticyclonic circulation that extends up to the sutropics.

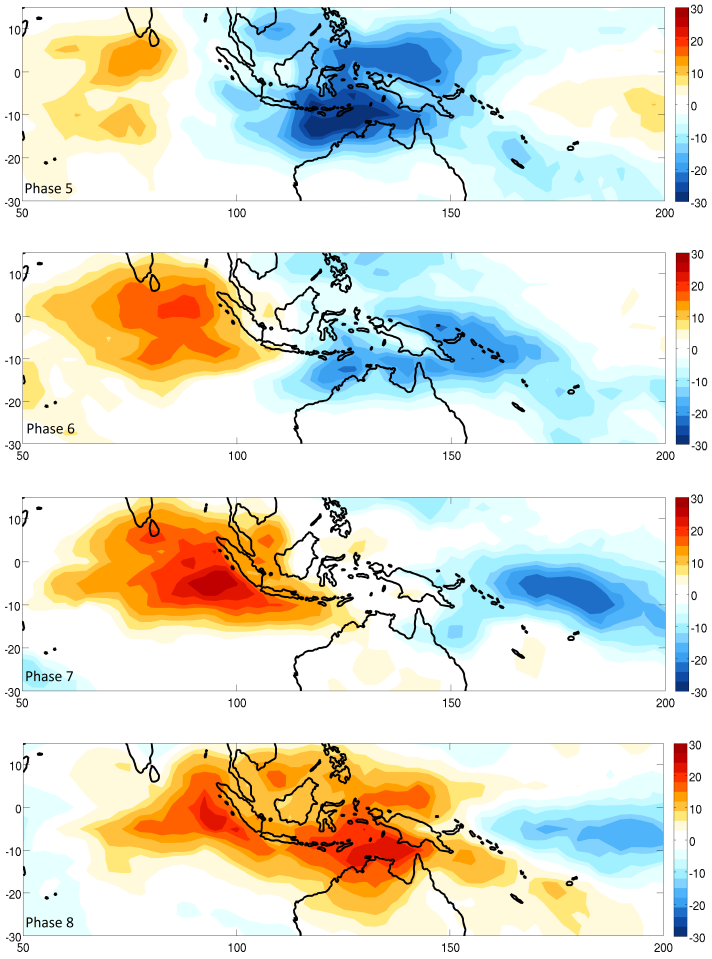

FIGURE 1.3 – Same as Figure 1.2 for MJO phases 5 to 8

Since the MJO affects many variables in the equatorial band, Wheeler and Hendon (2004) have developed a set of two indices describing the state of the MJO for each day. These two indices, named RMM1 and RMM2 (for Real-time Multivariate MJO index) are computed with a multivariate Principal Component Analysis (PCA) that includes OLR and zonal wind at two pressure levels, 850 hPa and 200 hPa, averaged over a near-equatorial band. For a given day, the two values in the phase space $(RMM1, RMM2)$ enable to distinguish between 8 phases of the MJO and to assess the strength of the MJO event. If $\sqrt{RMM1^2 + RMM2^2} < 1$, it is considered weak MJO. Otherwise, the day is classified in one of the eight MJO phases that indicates the position of the zone of enhanced convection. This is represented on Figure 1.4.

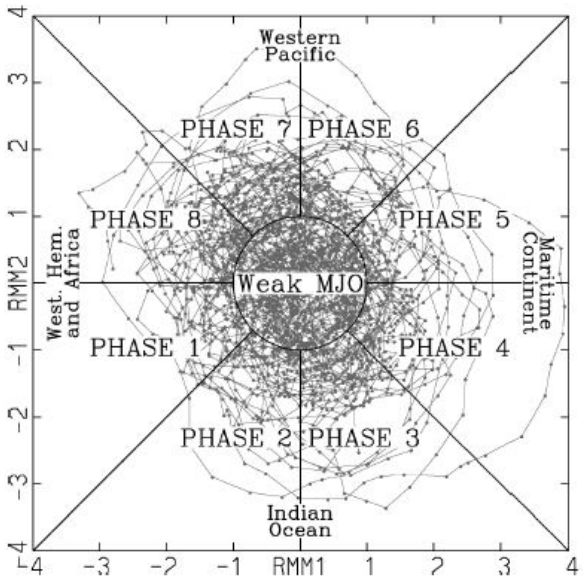

FIGURE 1.4 – Classification of days in the phase space of Real-time Multivariate MJO indices 1 and 2 (from Wheeler and Hendon (2004))

1.2 The diurnal cycle in tropical islands

Previous studies have highlighted some features of the diurnal cycle over tropical islands and its impact on precipitation. They all rely on the difference in heat capacity between land and sea. During the day, the island heats up and warms the air above, making the surface pressure decrease. The ocean remains colder and so does the air above it : in a classic situation, a horizontal pressure gradient between ocean and island appears, the air flow converges on the island and creates uplift motion that might lead to precipitation. During the night, land cools down more than sea and becomes colder than it, so the process reverses. This is the basic mechanism of land-sea breeze.

In an idealized model experiment of a flat, circular, low heat-capacity island, Cronin et al. (2015) have proposed a mechanism involving the diurnal cycle and explaining why islands were rainier than the surrounding ocean : the convergence of sea-breeze fronts is responsible for the formation of low-level clouds around noon, before these shallow clouds start forming deeper precipitating convective cells in the afternoon that eventually merge together and converge in the center of the island, triggering off heavy rainfall in late afternoon or early evening. Evidence of this process over real islands in the Maritime Continent is also shown in Qian (2008), who suggests the implication of this merging phenomenon, called the cumulus merger, to enhance precipitation. In night time, cloudiness over the island decreases and the diurnal signal propagates over the surrounding ocean due to gravity waves directed offshore (Yang and Slingo, 2001; Love et al., 2011) that intensify oceanic convection. Therefore, the island is most of the time rainier than the ocean, but this effect is modulated by the size of the island and its orography (Sobel et al., 2011) : the larger the island, the more rainfall and for large islands, a mountainous one is wetter than a flat one, primarily because of mechanical upslope air flow.

The best documented area for the diurnal cycle and its interaction with intra-seasonal to seasonal modes of variability is the Maritime Continent. The study by Love et al. (2011) mentioned above extensively describes the diurnal cycle in the Maritime Continent in a high resolution model and introduces its specific indicators, the time of maximum precipitation and the diurnal amplitude, that respectively quantify the phase and the intensity of the diurnal cycle. With the use of satellite preci-

pitation data (TRMM) and the index provided by Wheeler and Hendon (2004), Peatman et al. (2014) have illustrated the propagation of the MJO over the Maritime Continent and studied its impact on the diurnal cycle of precipitations in terms of amplitude and phase. They come to the conclusion that 80 % of the modulation of precipitation with the MJO is done through changes in the amplitude of the diurnal cycle. They also notice that the amount of precipitation and the diurnal cycle is affected with a positive lag, before the main MJO convective envelope reaches the zone.

With the use of circulation weather types as intermediary tools, Moron et al. (2015b) have also managed to link two dominant modes of variability (the Madden-Julian oscillation and the El Niño Southern Oscillation) to the diurnal cycle over islands of the Maritime Continent, basing their findings first on statistical relationships between the modes of variability and the distribution of their weather regimes, and then on the impacts of each weather regime on the diurnal cycle. The same approach is used by Qian et al. (2013) for the diurnal cycle of precipitation over Borneo in the monsoon period.

1.3 Climate and rainfall variability over New Caledonia

Compared to the Maritime Continent, rainfall over Pacific islands in general and over New Caledonia in particular has been under less scrutiny so far. One of the most extensive works remains the report by Leroy (2006) about seasonal forecasting in New Caledonia that reviews the main sources of climate variability in the country at intra-seasonal to interannual time scales, (including the MJO and ENSO) and their links to weather regimes in the area. This study focuses on the impact on temperature and precipitation, but does not go into the study of the diurnal cycle. As for weather regimes, Lefèvre et al. (2010) have developed a classification of four circulation types for the warm season, based on high-resolution surface winds provided by the QuickSCAT satellite, and have been able to link them to the large-scale modes of variability in the Pacific. This paper also highlights the crucial interaction between low-level atmospheric circulation and the orography of New Caledonia. In terms of rainfall, Barbero and Moron (2011) have studied the impact of interannual to decadal large-scale climate variability on New Caledonia precipitation. For shorter time scales, Moron et al. (2015a) have used a method of Hidden Markov Models to rain gauge data in the archipelago in order to classify the days in six rainfall states, that are then linked to subseasonal variability and ENSO. So far, there are no studies linking the diurnal cycle of New Caledonian precipitation to intra-seasonal time scales.

Data

2.1 Precipitation data

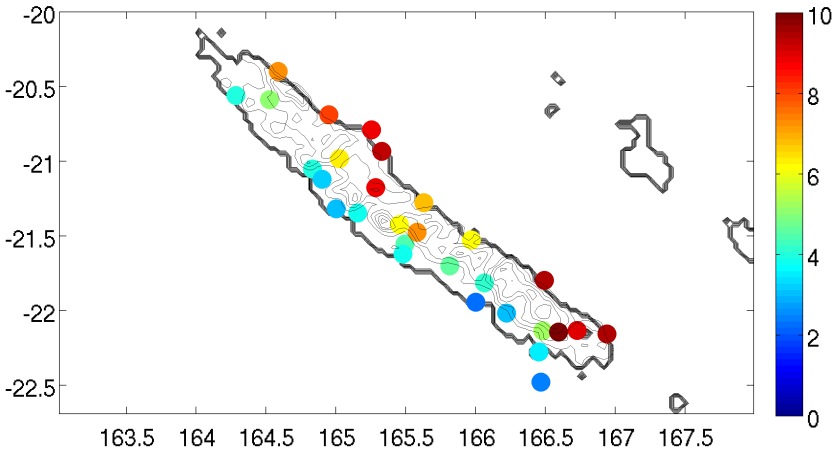

FIGURE 2.5 – Location of the 29 rain gauges stations and average precipitaton (mm/day) over the warm seasons (November-April) of the 1991-2014 period

Studying the diurnal cycle of precipitation requires to have high-frequency rainfall data over the Caledonian area, with several measurements per day. The main product we used for this is the record of rain gauge data provided by Météo France in New Caledonia, based in Nouméa. We restricted ourselves to a set of 29 rain gauges distributed all across the Mainland with hourly resolution (see list in Appendix 1, Table 8.8). The time period available changes depending on the meteorological station, so we chose a study period covering 24 years, from January, 1st, 1991 to Decembre, 31st, 2014. The location of the 29 rain gauge stations can be seen on Figure 2.5, along with the average precipitation for New Caledonia warm season (November-April). It can be noted that the rainiest areas are the East coast and the central mountain range, along with a few stations in the south of the Mainland, where there is also a dam and a large lake (Yaté lake). In addition to that, we also looked into the TRMM 3B42 version 7 satellite precipitation data, from January, 1st , 1998 to December, 31st , 2014 with a 3-hour temporal resolution and a 0.25° spatial resolution. It is freely available online and we downloaded it from the Live Access Server `http://apdrc.soest.hawaii.edu/las8/UI.vm` on the spatial domain 140°E-180°E and 35°S-0°. Given that the time is given in UTC, we had to account for New Caledonia time zone (UTC +11 h). However, owing to the poor performance of the TRMM data to capture land precipitation (that were hugely underestimated) and its low resolution, we did not go into further investigation with this product.

2.2 Wind data

There are several possible wind fields for the determination of synoptic circulation regimes. Lefèvre et al. (2010) used the high-resolution 0.125° QuickSCAT winds over New Caledonia, while Moron et al. (2015b) used the 850 hPa horizontal wind field provided by the NCEP2 (National Center for Environmental Prediction) reanalysis. Here, we chose to use a freely available product called Blended Sea Winds and provided by NOAA National Climatic Data Center. It is an ocean surface wind field (zonal and meridional) with a 0.25° spatial resolution, available every day from July, 9th ,1987 to present. It is reconstructed from various satellite wind data (including the QuickSCAT data) that give the wind speed, and the direction of the winds is provided by the NCEP2 reanalysis. This product is presented by Zhang et al. (2006) and on the website `https://www.ncdc.noaa.gov/oa/rsad/air-sea/seawinds.html` from where it can be downloaded. We retrieved this wind data for the 1991/01/01 to 2014/12/31 period and on the spatial domain 150°E-18°E and 35°S-10°S.

2.3 Reanalysis data

In order to look at some basic variables on a large domain around New Caledonia, we used NCEP2 atmospheric reanalysis data, accessible on the Live Access Server `http://apdrc.soest.hawaii.edu/las8/UI.vm`. This reanalysis runs from 1979/01/01 to present, and is described in Kanamitsu et al. (2002). The data was retrieved on the same domain 150°E-180°E/35°S-10°S and includes variables such as Sea Level Pressure (SLP), zonal and meridonal wind at 10 m above surface, or even zonal, meridional and vertical winds at various pressure levels.

2.4 Model data

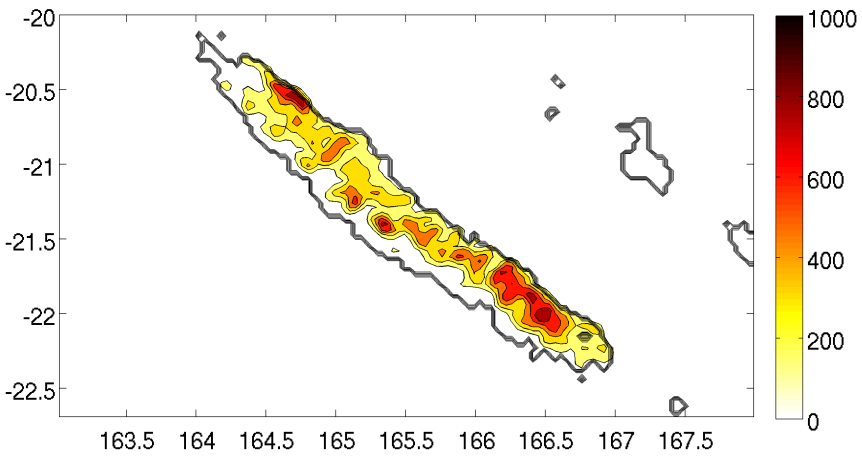

FIGURE 2.6 – Altitude in the WRF 2.2 model simulation (m)

A 4-km atmospheric model experiment was simulated on the domain 161°E-170°E and 25°S-17°S (165 x 165 points in longitude-latitude), centered on New Caledonia, with the atmospheric model WRF (Weather Research and Forecasting), version 2.2. The details of the setting of the model are given in Lefèvre et al. (2010), but the following facts deserve to be highlighted : convection is represented by Betts-Miller-Janjic cumulus parametrization, the model was forced by the 6-hourly NCEP operational analysis (NCEP-FNL) and the orography is provided by New Caledonia Remote Sensing and Geomatics Services (DTSI). Owing to orography smoothing, although the main features of the mountain range are represented, there is some reduction of peaks and filling of valleys. As a result, the 4-km resolution

model is unable to resolve the orography variance below 20 km. The orography considered by the model is represented on Figure 2.6. Note that the highest mountains peaking at approximately 1600 m in reality (Figure 1) are smoothed down to about 1000 m in the model. The time period of the simulation extends from November, 1st, 2008 to May, 30th, 2014, and the model output was recorded at hourly intervals, accounting for New Caledonia time zone UTC +11 h.

2.5 Madden-Julian oscillation phases

The two Real-time Multivariate MJO indices defined by Wheeler and Hendon (2004) are provided for every day from June, 6th, 1974 to present, along with the MJO phase (from 1 to 8) and the MJO amplitude $\sqrt{RMM1^2 + RMM2^2}$, on the website
http://www.bom.gov.au/climate/mjo/graphics/rmm.74toRealtime.txt. These values are computed with OLR data from NOAA satellites and zonal wind values at 850 and 200 hPa from NCEP reanalysis. A more precise description can be found at http://www.bom.gov.au/climate/mjo/. Using these MJO phases, it is possible to compute the average daily precipitation for each phase, and spatially average it on all stations. This is represented on Figure 2.7, which shows that the rainiest MJO phases for New Caledonia are phases 5,4 and 6, while the driest are phases 1 and 2. This seems to be roughly consistent with the location of the MJO-induced zone of enhanced equatorial convection. Indeed, in Wheeler and Hendon (2004), phases 4 and 5 are associated to a positive anomalous convective patch over the Maritime Continent and phase 6 corresponds to a location of the patch in the Western Pacific (see Figure 1.4). Other composites of New Caledonia rainfall on MJO phases can also be vizualized in Appendix 1 (Figure 8.34) and Appendix 2 (Figure 8.35) on Météo France and TRMM data.

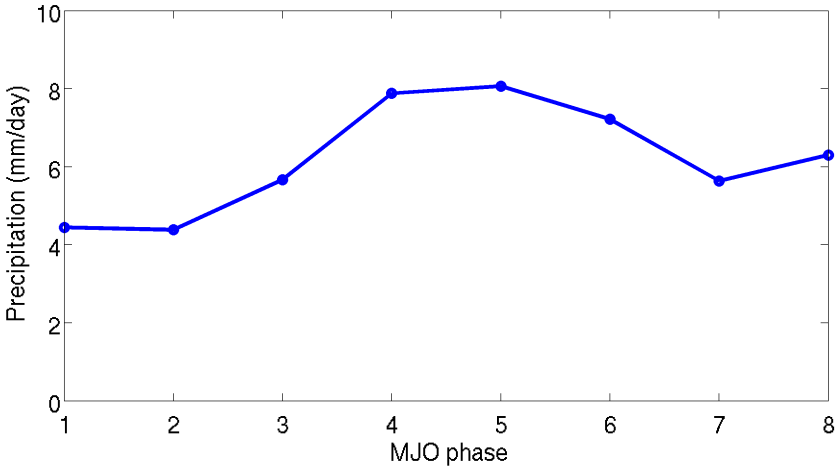

FIGURE 2.7 – Evolution of mean precipitation (mm/day) averaged over the 29 stations with the MJO phase

Determination of weather regimes

3.1 Methodology

We selected the daily wind fields of Blended Sea Winds for the 24 warm seasons in the period 1991/01/01-2014/12/31, which makes 4350 days (181 or 182 days per warm season, depending on bissextile years). After trying several possibilities in terms of box sizes, we restricted the area of determination to the domain 161°E-170°E and 25°S-17°S, because it was sufficiently small to capture different circulation patterns over New Caledonia and sufficiently large to give also different circulation patterns at larger spatial scales. The method for determining these weather regimes is similar to that used by Moron et al. (2015b) and Lefèvre et al. (2010), among others.

At each grid point, standardized anomalies of zonal and meridional winds were computed by subtracting the mean on the whole period (the 24 warm periods) and by dividing by the standard deviation. They were also weighted by the square root of the cosine of the latitude so as to account for the smaller surface areas of grid cells at higher latitudes. Then, Principal Component Analysis (PCA) was performed on the multivariate data : for each time step, zonal and meridional wind anomalies were appended next to each other. The eigenvectors and eigenvalues of the covariance matrix gave the Empirical Orthogonal Functions and the associated variance. The space dimension was reduced by keeping only the 18 first EOFs, accounting for about 95 % of the total variance. Each day had its coordinates, the 18 first principal components, in the subspace of the 18 EOFs.

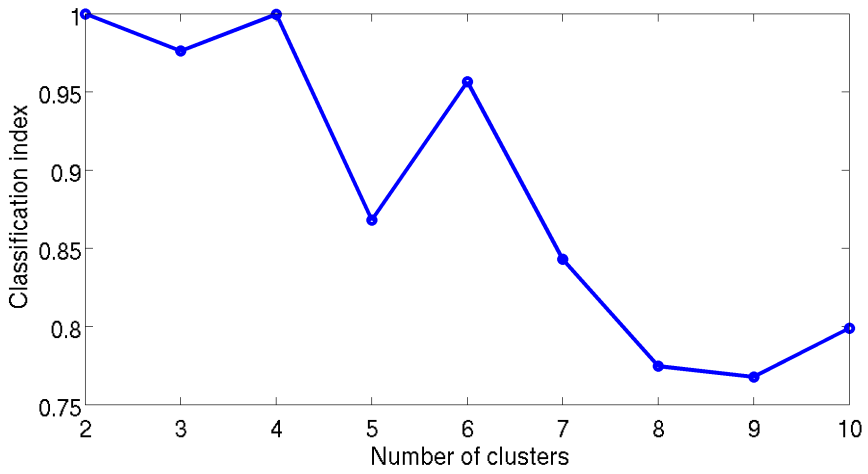

FIGURE 3.8 – Classifiability Index (CI) on Blended Sea Winds 1991-2014 warm season days, as defined by Michelangeli et al. (1995)

These 4350 days were classified using a k-means clustering algorithm. In this study, we used the k-means clustering function proposed by the software MATLAB. This clustering algorithm requires to specify the number k of clusters chosen and sorts out all the days into k clusters. The clustering algo-

rithm chooses randomly k initial seeds as cluster centroids and groups all days into one of these clusters depending on which seed is the closest. The next step takes the centroids of each of the newly-formed k clusters as the new seeds, and the process is iterated until the intra-cluster variance is minimized and the inter-cluster variance is maximized. The trouble is that the distribution in the final k clusters depends on the initial seeds. This is why we must choose a number of clusters k such that the clusters given by the algorithm do not depend too much on the initial seeds. In other words, the data must be classifiable into the number of clusters chosen.

In order to determine the number of clusters k, we used the classifiability index (CI) defined by Michelangeli et al. (1995). For each number k from 2 to 10, 50 different partitions of our data were computed using the MATLAB k-means algorithm. Then, the similarity between two partitions was evaluated as the smallest of all correlations between the pairs of corresponding centroid wind maps. Averaging all the similarities between the 50 partitions gives a classifiability index CI associated to the number of clusters k. CI is comprised between 0 and 1, 1 meaning that all partitions in k clusters give identical results. Figure 3.8 shows the CI of our wind data for a number of cluster k from 2 to 10. The number of clusters that is eventually chosen must have a classifiability index sufficiently close to 1 for robustness, but it must be adequate with the number of synoptic situations that we want to analyze. In this case, we retained 4 weather regimes as the best option, instead of two for instance, because two regimes would not capture enough diversity in synoptic circulation. This number seems consistent with other studies (Leroy, 2006; Lefèvre et al., 2010) in which four regimes were also found out using other methods.

3.2 Weather regime composites on NCEP2 SLP and surface winds

Regime	Easterly	Southerly	Trades	Northerly	**Total**
Number	1460	778	1457	655	4350
%	33.6	17.9	33.5	15.1	100

TABLE 3.1 – Distribution of the warm season days 1991-2014 between the four weather regimes

The number of occurrences for each regime can be found in Table 3.1. Figures 3.9 and 3.10 show the maps of the four warm season weather regimes composites for NCEP2 SLP (Sea Level Pressure) and 10 m wind on a domain that is larger than the determination domain (in the rectangle). The first regime corresponds to easterly wind over New Caledonia, with a high pressure zone in the southeast of the big domain, over the Kermadec archipelago. The second regime represents a southerly flow associated with a low pressure zone to the East of New Caledonia. The third regime is the southeasterly flow commonly known as the trade wind regime. Finally, the fourth regime corresponds to a northerly flow associated with a very low pressure zone closely to the west of New Caledonia. Although these regimes are not exactly the same as the ones determined with other data product by Leroy (2006) and Lefèvre et al. (2010), some common features can be noticed such as the trade wind flow, the easterly regime or even the location of the depressions and anticyclones at a large scale.

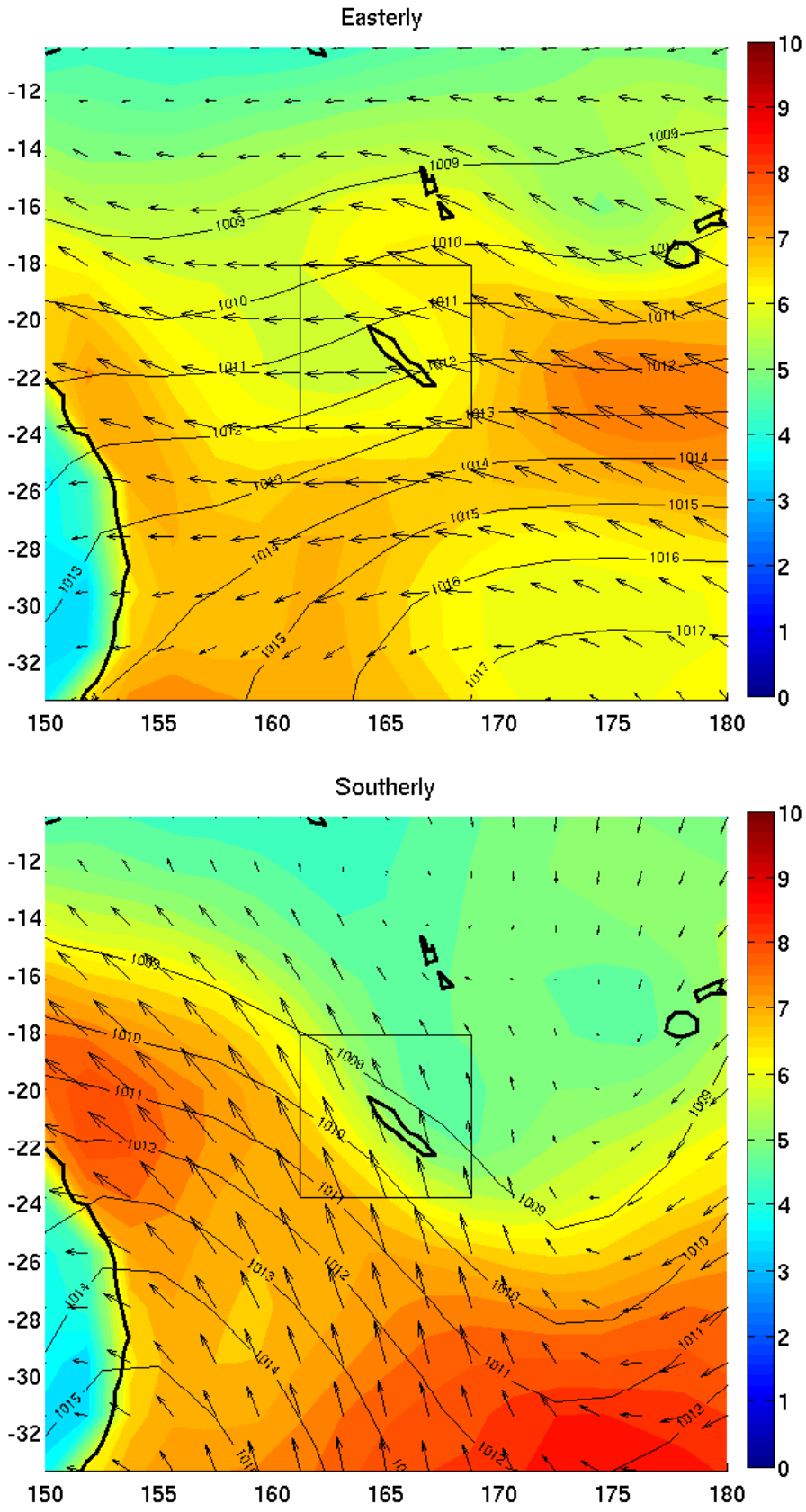

FIGURE 3.9 – Composites of 10-m wind (arrows), 10-m wind speed (filled contours, m/s) and SLP (contours, hPa) in NCEP2 reanalysis for easterly and southerly regimes. The rectangle represents the geographical domain on which the regimes were determined.

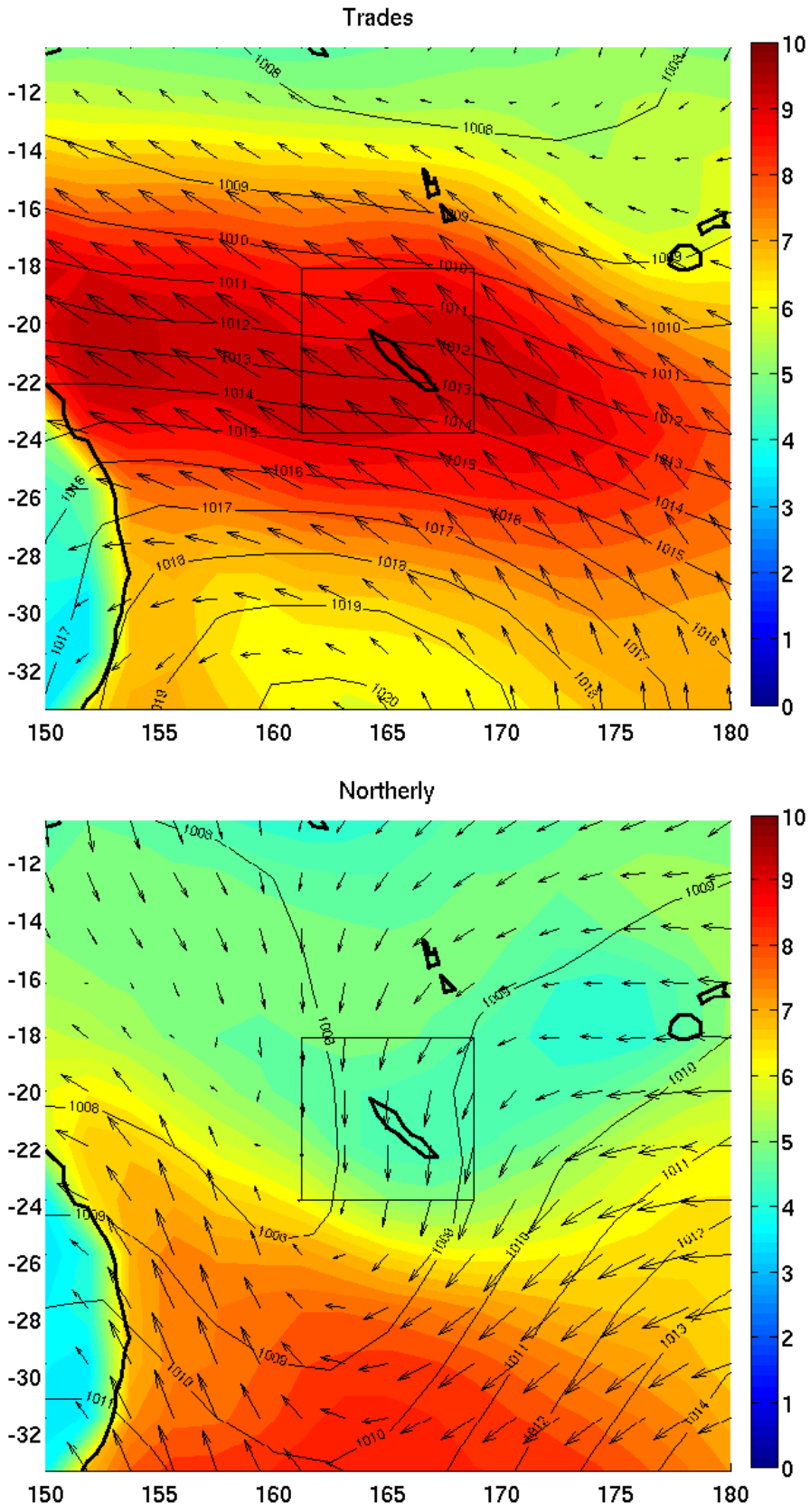

FIGURE 3.10 – Same as Figure 3.9 for trade and northerly regimes.

Weather regimes as a tool to study MJO impact

4.1 Statistical relationship between MJO and weather regimes

MJO phase		Easterly	Southerly	Trades	Northerly
1	O	81	22	46	97
	E	83	37	44	82
	R	-0.22	**-2.47**	0.30	1.66
2	O	140	26	28	105
	E	100	45	53	100
	R	**4.0**	**-2.83**	**-3.43**	0.50
3	O	164	41	47	148
	E	134	60	72	134
	R	**2.59**	**-2.45**	**-2.95**	1.21
4	O	167	48	48	115
	E	127	57	68	127
	R	**3.55**	-1.19	**-2.42**	-1.06
5	O	132	93	50	98
	E	125	56	67	125
	R	0.63	**4.94**	**-2.08**	**-2.41**
6	O	111	78	95	91
	E	126	56	67	126
	R	-1.34	**2.94**	**3.42**	**-3.12**
7	O	88	55	83	126
	E	118	53	63	118
	R	**-2.76**	0.27	**2.52**	0.74
8	O	78	47	66	103
	E	99	44	53	98
	R	**-2.11**	0.45	1.79	0.50
Weak	O	499	245	315	574
	E	548	246	292	547
	R	**-2.09**	-0.06	1.35	1.15
p-value		3.1e-9	2.10e-9	3.3e-9	1.2e-3

TABLE 4.2 – Result of the chi-square goodness-of-fit test between observed and expected days, assuming that the distribution of weather types does not depend on the MJO phase. O : observed. E : expected. R : Pearson's residual. In bold type, residuals that have an absolute value greater than 2.

Linking weather regimes and large-scale variability through statistics is commonplace, as can be seen in Moron et al. (2015b), Qian et al. (2013), Leroy (2006) or Lefèvre et al. (2010). One of the most simple evidence of a relationship between MJO and daily synoptic circulation can be provided by a chi-square test. We consider the classification of our $N_T = 4350$ days of warm season into the eight MJO phases plus the weak MJO days. For each of the four weather regimes, the null hypothesis states that the days of this regime are homogeneously distributed between the nine phases, accounting for the number of days of each phase in the time series. The null hypothesis gives an expected repartition of each weather regime between the MJO phases. This repartition is compared to the effective observed repartition through the chi-square indicator $\chi^2 = \sum_{i=1}^{j} \frac{(O-E)^2}{E}$ with O and E respectively representing the observed and expected numbers, $j = 9$ the number of phases. For a given phase ϕ_i and a given regime R_l, the expected number E is calculated as $E = N_{days}(l) \times \frac{N_{days}(i)}{N_T}$.

For each regime, the p value of the chi-square indicator is the image of the chi-square indicator by the chi-square probability density function with eight degrees of freedom (9 phases -1). The p-value gives the probability that a random distribution gives a chi-square value larger than the one obtained. In other words, it assesses the probability that the discrepancy between the observed and expected values is larger than the one we get considering the null hypothesis. A criterion commonly used to reject the null hypothesis is the 95% criterion, that is to say when the p-value is smaller than 0.05. As we can see in Table 4.2, it is true for every regime, which highlights the fact MJO and weather regimes are linked. Knowing the phase for which a given regime is over-represented or under-represented is possible with Pearson's residuals $R = \frac{O-E}{\sqrt{E}}$ that also appear in Table 4.2. A common "rule of thumbs" can be used : if the residual is greater than +2, the regime is over-represented in the given phase and it is under-represented if the residual is less than -2.

MJO phase	Total	1	2	3	4	5	6	7	8	Weak
Easterly	33.6	32.9	**46.8**	**41.0**	**44.2**	35.4	29.6	*25.0*	*26.5*	*30.6*
Southerly	17.9	18.7	*9.4*	*11.7*	*12.7*	*13.4*	**25.3**	**23.6**	22.4	19.3
Trades	33.5	39.4	35.1	37.0	30.4	*26.3*	*24.3*	35.8	35.0	35.1
Northerly	15.1	*8.9*	*8.7*	10.2	12.7	**24.9**	**20.8**	15.6	16.0	15.0

TABLE 4.3 – Percentage of weather regimes by MJO phase. Bold type : the regime is over-represented in the MJO phase relative to the total. Italics : the regime is under-represented in the MJO phase relative to the total. Note that each column adds up to 100 %

Using residuals, Table 4.3 shows the percentage of days represented by each regime in the total number of days and in each MJO phase. A striking fact is that the easterly flow regime is over-represented during MJO phases 2,3 and 4 that are phases of suppressed convection for New Caledonia. On the contrary, the northerly regime is over-represented during the convectively active phases 5 and 6 and under-represented in the phases of suppressed convection 1 and 2. By the way, this is consistent with the fact that phases 5 and 6 are the rainiest phases and the northerly regime is the wettest regime. As for the southerly regime, it is over-represented at the end of the active MJO in phases 6 and 7, while it is under-represented before. Finally, the trade wind regime is more evenly distributed between the phases, although it is under-represented in the phases of active convection 5 and 6. This tends to suggest that during the propagation of a MJO event, the winds blowing over New Caledonia tend to align as easterly winds, before turning northerly when the active MJO envelope arrives, and eventually becoming southerly after the passage of the envelope.

4.2 Dynamical relationship between MJO and weather regimes

In order to investigate the hypothesis stated above, the anomalies in the 10 m wind field in the NCEP2 reanalysis at 2.5° resolution were plotted along with the OLR anomalies representing the propagation of the MJO (Figures 4.11 and 4.12). The propagation of the MJO in the eight phases comes along with a change in the orientation of the wind field anomalies in New Caledonia area. The southeasterly anomalies that are noticeable in phase 1 start rotating counter-clockwise with the propagation of the MJO, bringing a succession of easterly (phases 2 and 3), northerly (phases 5 and 6) and southerly (phase 7) anomalies. Of course, the orientation is not exactly the same as the one in our regime composites because as we can see on Table 4.2, a single MJO phase can be associated with any of the four different synoptic situations depending on the day.

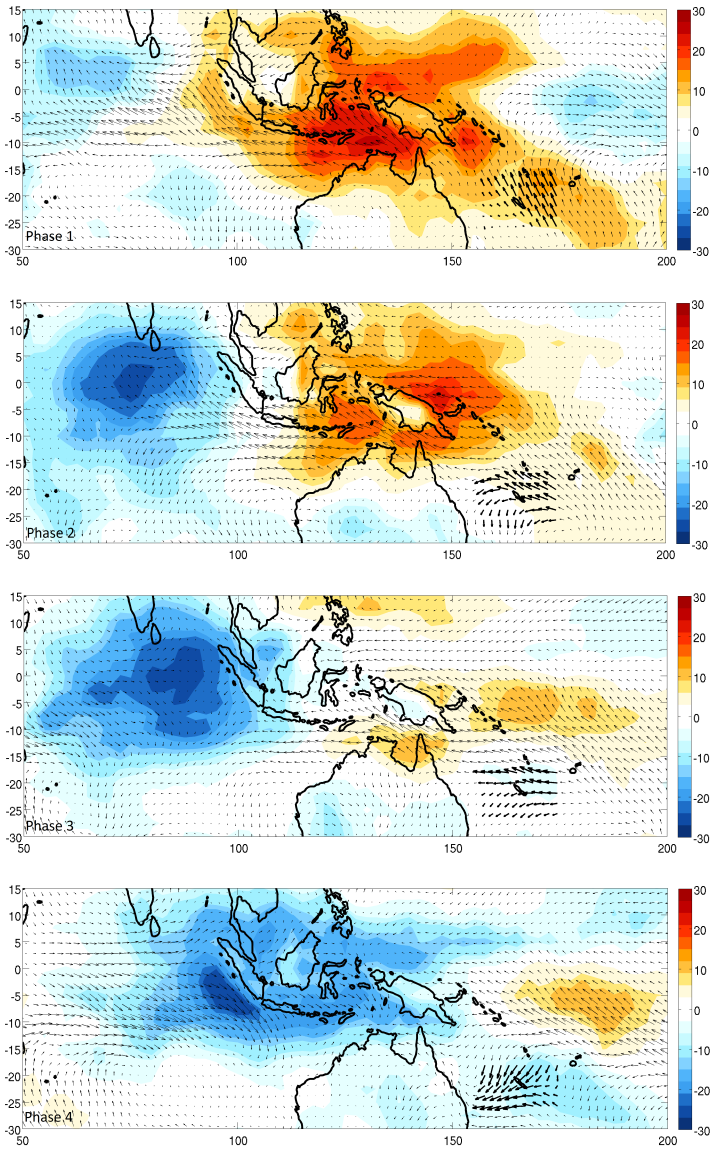

FIGURE 4.11 – Outgoing Longwave Radiation (OLR) anomalies OLR [a] in W/m^2 (as defined in Wheeler and Hendon (2004)) and 10 m wind anomalies in NCEP2 reanalysis for MJO phases 1 to 4. Negative OLR anomalies : enhanced convection. Positive OLR anomalies : suppressed convection.

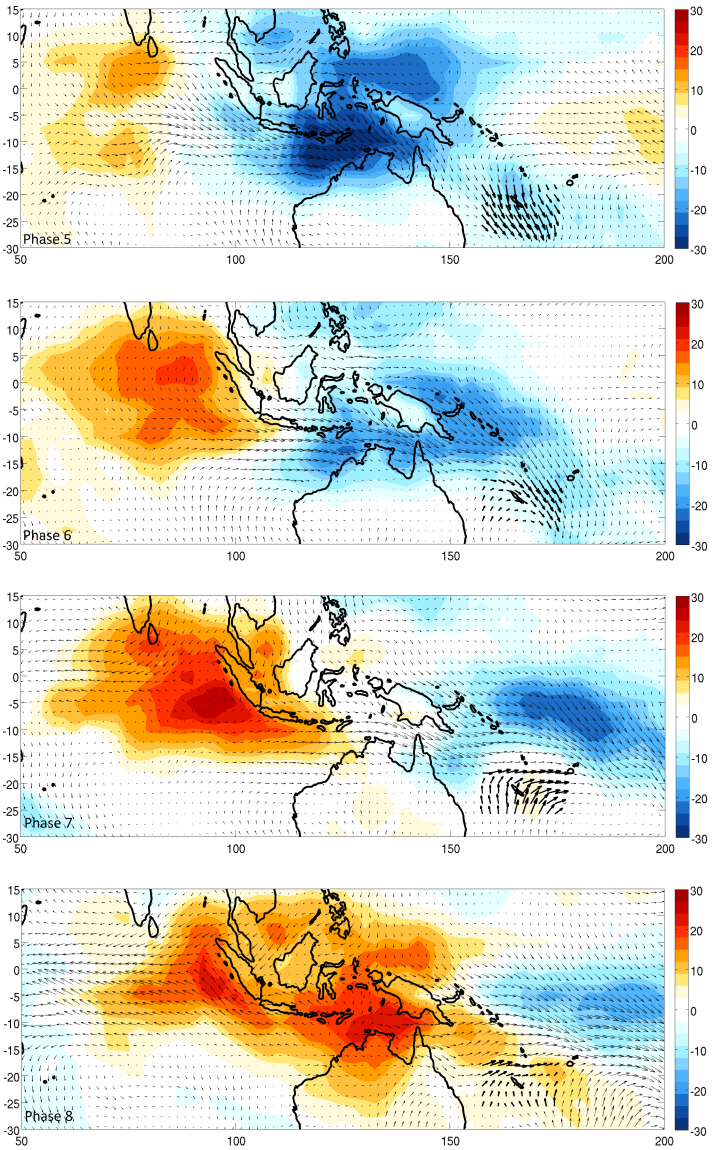

FIGURE 4.12 – Same as Figure 4.11 for MJO phases 5 to 8

A physical explanation of the effect of MJO equatorial propagation on large-scale circulation in the subtropics can be found out in Rui and Wang (1990), following the theoretical model proposed by Gill (1980). A deep convection patch in the tropical band is responsible for diabatic heating. This creates a low-pressure zone that favors convergence of winds at the surface. Due to Coriolis deflection, cyclonic gyres form at the surface near the convection center on both sides of the equator. The convection center is therefore responsible for a change in the position of cyclonic and anticyclonic circulations that has an impact up to the subtropics. When this convection center is displaced with MJO propagation, the cyclonic gyres move along. The position of New Caledonia in the low subtropics (20°S) makes it sensitive to MJO convection anomalies indirectly, through circulation anomalies, rather than directly. Between phases 5 and 7, depending on the location of the convective center, it is either located in the northward or southward branch of the cyclonic gyre. In phases 2 to 4, it is located in a zone of anticyclonic anomalies that are responsible for easterly flow. Yet, Figures 4.11 and 4.12 also show that during the phases when the convective center is the closest (5 and 6), convection is also intensified above New Caledonia, which is still close enough to the equator to be directly impacted by MJO-induced convective anomalies. However, this effect might be secondary compared to the circulation anomalies that bring moist or dry air depending on the place where the synoptic winds come from.

Spatial classification of the rain gauge stations

5.1 Methodology

For each of the 29 stations, the 24 time step composite diurnal cycles for each of the four weather regimes were concatenated one next to each other, giving a 29 by 96 matrix. These composite diurnal cycle had previously been filtered by keeping only their mean value and their three first harmonics using Fast Fourier Transform (FFT). Ascendant Hierarchical Clustering (AHC) was calculated on the rows of the 29 by 96 matrix in order to classify the stations. The metric used was correlation and the distance between clusters was computed using Ward's minimum variance method. In this algorithm, the similarity between two stations is evaluated by the correlation between their diurnal cycles. At the beginning, each station represents a cluster of its own. The process is iterated by merging the two closest clusters into one bigger cluster. This can be represented on a hierarchical clustering tree called dendrogram, on Figure 5.13.

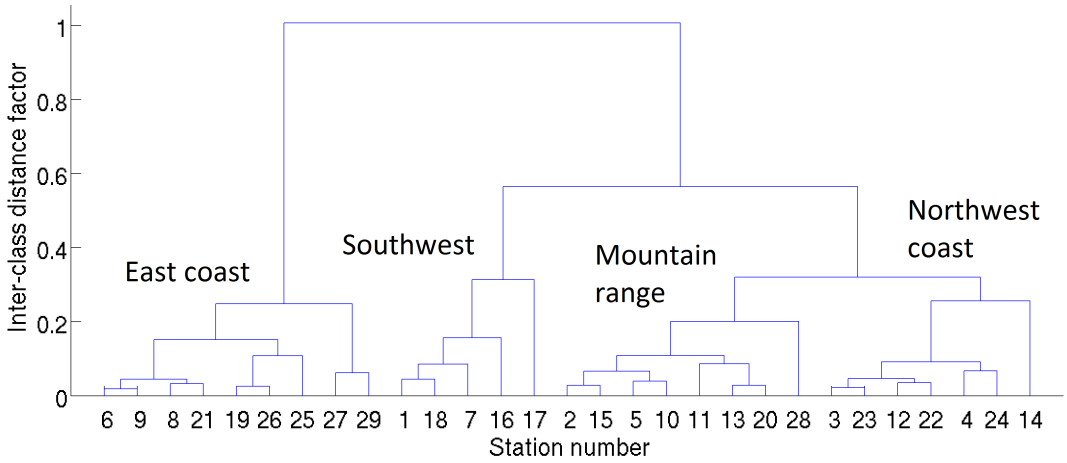

FIGURE 5.13 – Dendrogram of the Ascendant Hierarchical Clustering of the 29 stations. The four groups corresponding to the four clusters retained are indicated.

5.2 Rain gauge clusters

The number of station clusters chosen depends on the number of geographical zones that we want to distinguish and for which we will be able to provide physical interpretations. In this case, we retained four geographical zones that are represented by the colored dots on Figure 5.14. Cluster 1 corresponds to the stations located on the main axis of the Mainland, on the mountain range. It will be called "Range" herafter. Cluster 2 is composed of stations on the northwest coast, called "Northwest" he-

reafter. Cluster 3 corresponds to a group of 5 stations, called "Southwest" hereafter, that all have in common a big variability in their diurnal cycle depending on the weather regime, most of the time with more noise than in other clusters. Finally, Cluster 4, hereafter called "East", groups together all East coast stations.

This number of geographical clusters can be justified by the sufficient number of stations in each cluster (5 at least) and by the easy link that can be made between each cluster and a specific geographical zone. Considering the dendrogram (Figure 5.13), the most evident distinction (2 clusters) that the algorithm is able to make is between the East coast and all the other stations. Then, if the number of clusters is set to three, the 5 stations from the Southwest zone separate from the remaining stations, that form a big group with the stations in the mountain range on the one hand and the stations on the northwest coast on the other hand. In other words, the two closest groups in terms of diurnal variability with weather regimes are the mountain range and the northwest coast, that are therefore expected to show a similar behavior.

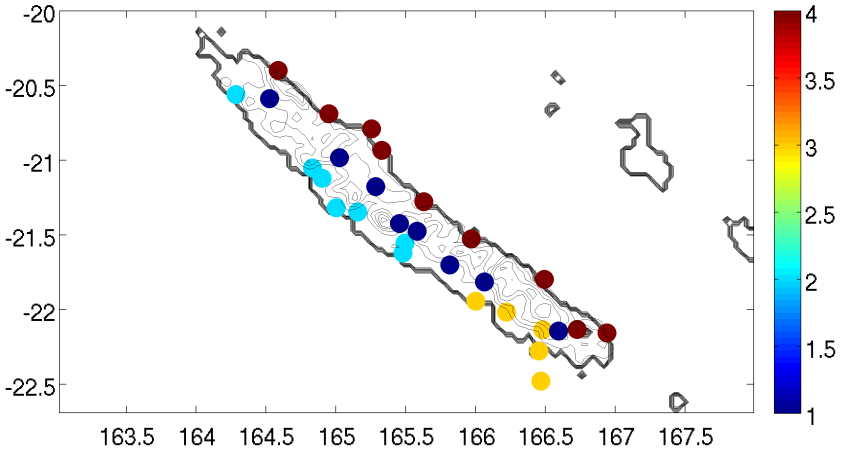

FIGURE 5.14 – Classification of the 29 rain gauge stations in 4 clusters. The color represents the index number of the cluster.

Analysis of the diurnal cycle of precipitation

6.1 Average rainfall and diurnal cycle for each weather type

Figure 6.15 represents the composite diurnal cycles of precipitation averaged over all 29 Météo France stations for each regime. It can be noticed that the northerly regime is by far the wettest in terms of average rainfall, followed by the easterly and southerly regimes. On the contrary, the trade wind regime is the driest. Diurnal variations remain similar in average for all regimes, with a precipitation peak around 03 :00 PM Local Time (LT), but the amplitude of diurnal variability increases in concert with the average rainfall amount. We may also notice that the northerly regime is characterized by a secondary peak during the night around 02 :00 AM. The average diurnal cycle with a rainfall peak in the afternoon will be called the standard diurnal cycle hereafter.

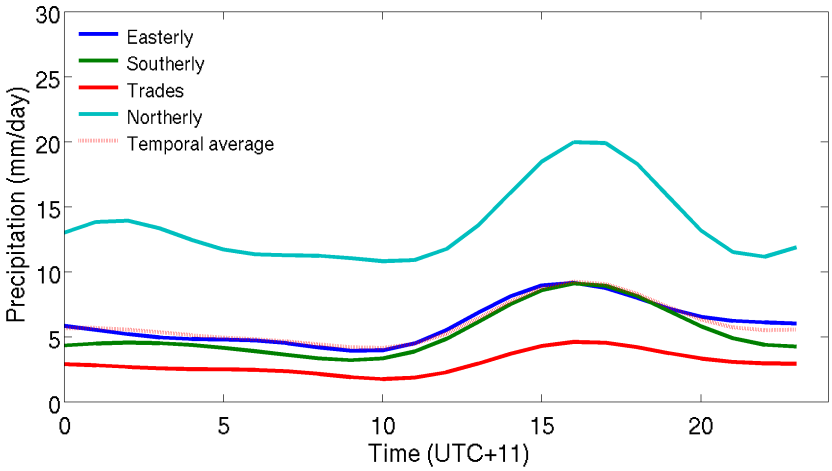

FIGURE 6.15 – Average diurnal cycle of precipitation (mm/day) on the 29 stations for each weather type

6.2 Average rainfall and diurnal cycle for each spatial cluster

Without considering any distinction of weather type, the diurnal cycles averaged over all days and all stations belonging to the same clusters are shown in Figure 6.16. The diurnal cycle has the general shape of the standard average diurnal cycle in 3 out of the 4 clusters, namely the mountain range, the northwest coast and the southwest zone. The amplitude of the afternoon peak is conditioned by the average precipitations and is larger in rainier area. The mountain range is the rainiest while the southwest zone is the driest, with a "flatter" diurnal cycle. As for the East coast, it is roughly as rainy as the mountain range in terms of daily average but shows a completely different diurnal cycle : the

amount of rainfall reaches a minimum at the end of the morning and starts to go up again, reaching a maximum in the afternoon around 03 :00 PM and keeping this high level of precipitation until the middle of the night, around 02 :00 AM. The amplitude of such a diurnal cycle is also smaller than that of the standard diurnal cycle that is recorded in other areas and in average. This will be called the non-standard East coast diurnal cycle.

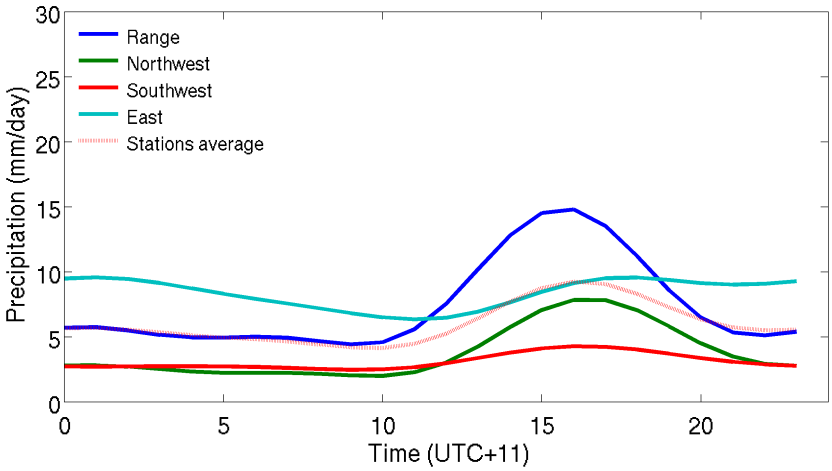

FIGURE 6.16 – Diurnal cycles of precipitations (mm/day) averaged on each geographical zone

6.3 Geographical impact of each weather regime

As the stations were classified on the variability of their diurnal cycle with the synoptic circulation, it is important to observe the diurnal cycle for each spatial cluster and for each regime. In Figure 6.17, the striking point about the diurnal cycle in the mountain range is that it always corresponds to the standard diurnal cycle whatever the regime, following the hierarchy in the four weather types in terms of rainfall amounts and amplitude of the peak.

The northwest coast (Figure 6.17) exhibits a similar behavior, with less rainfall though, in most cases : only the southerly wind regime is responsible for a "flatter" diurnal cycle with two small peaks at the end of the night and at the end of the afternoon. It should be underlined that the southerly regime is the only one for which the northwest coast is on the windward side of the mountain range.

The southwest zone (Figure 6.18) shows quite a variable diurnal cycle which really depends on the orientation of the dominant winds. In case of a trade wind regime, there is basically no diurnal cycle, while it is close to a standard diurnal cycle in case of northerly or easterly winds. The southerly regime also entails a particular behavior on this zone, with a two-peak diurnal cycle but no strong variability as a whole.

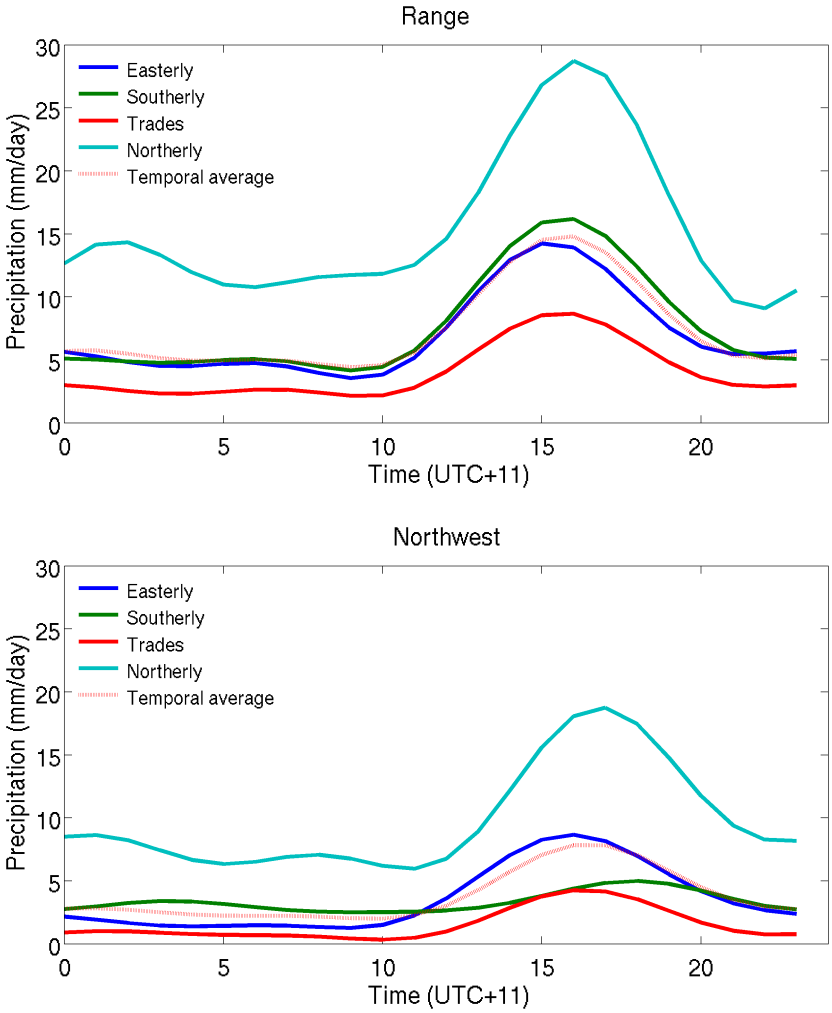

FIGURE 6.17 – Diurnal cycles of precipitation (mm/day) for geographical zones Northwest and Range and for each weather regime

Finally, the East coast (Figure 6.18), for which we have seen before that it has the most particular behavior, is impacted similarly by the trade regime and the easterly regime, with a minimum in the late morning and a maximum around midnight. This diurnal cycle is close to its average diurnal cycle represented in Figure 6.16. However, the northerly and southerly regimes both have particularities : high average precipitation with two peaks for the northerly regime, and a surprisingly standard diurnal cycle for the southerly winds. As we mentioned before, the southerly regime is the only wind regime for which the West coast is on the windward side in relation with the mountain range axis, but as a result it is also the only one for which the East coast is located on the leeward side. Therefore, it turns out that when located on the leeward side, the non-standard East coast diurnal cycle becomes standard and similar in shape to the ones that can be observed elsewhere, with a peak in the afternoon. In the meantime, southerly winds seem to entail less diurnal variability of precipitation on the West coast than usual.

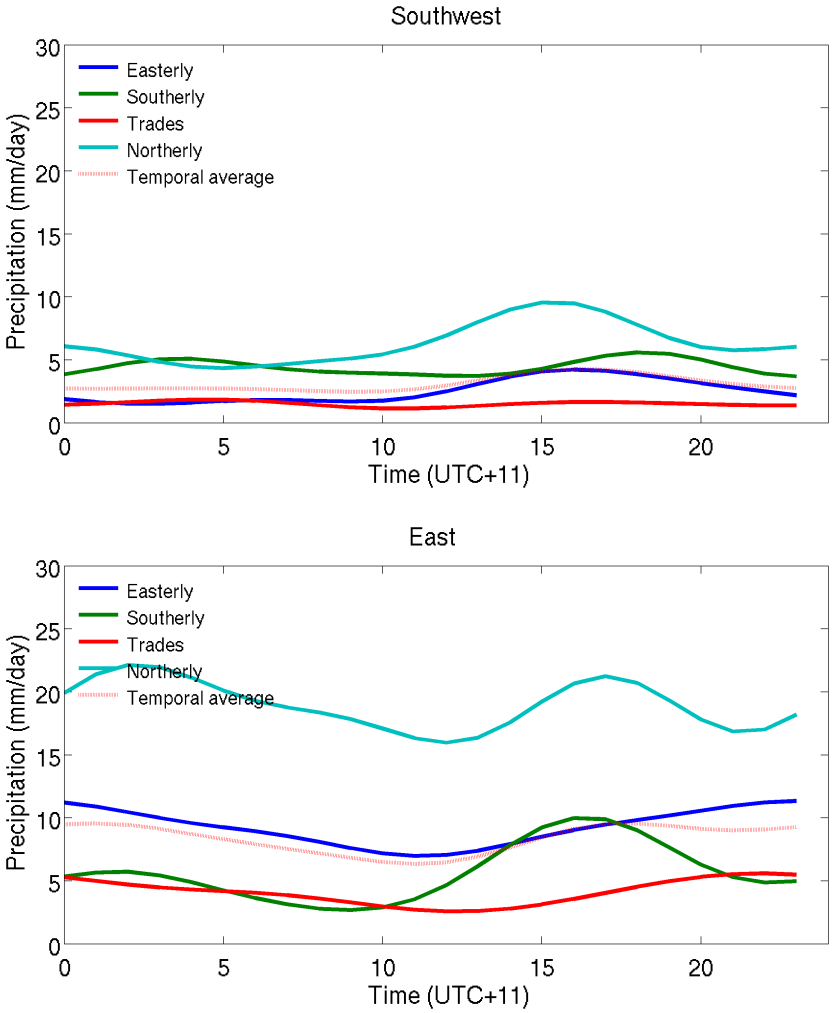

FIGURE 6.18 – Same as Figure 6.17 for geographical zones Southwest and East

After this descriptive approach of the variation of the diurnal cycle of precipitation relative to the geographical location and synoptic winds, trying to provide explanations for the observed behaviors comes naturally as the next step. This requires to go deeper into the underlying physical mechanisms that might affect rainfall variability. Considering that the number of physical quantities that are accessible to observations is limited, one of the most common approach when attempting to explicit such mechanisms is to analyze a model simulation output that is able to provide more variables, and often at a better resolution. We will therefore look into the diurnal cycle of precipitation and the phenomena that influence it in the WRF 2.2 simulation mentioned in Section 2.4.

The diurnal cycle of rainfall in a model simulation

7.1 Determination of weather regimes

The same methodology as in Section 3.1 was applied to determine circulation regimes in the model output data, based on the values of the zonal and meridional wind at 10 m above surface. Hourly values were averaged for each day (in New Caledonia time zone) and the 1086 days of warm season (November-April) comprised between November, 2nd, 2008 and May, 30th, 2014 were classified using the k-means algorithm after choosing a convenient number k of clusters. From Figure 7.19 that represents the values of the classifiability index for partitions between 2 and 10 clusters, one would tend to select 5 clusters. Yet, after trying for 4 and 5 clusters, it could be noted that 2 of the 5 clusters were similar in terms of wind direction, while the four clusters were all very distinct and alike the ones obtained with Blended Sea Winds. Then, in order to be able to make the comparison between these regimes and the previous ones, we retained the value of 4 clusters again, deeming that a classifiability index close to 0.9 was satisfying enough for robustness.

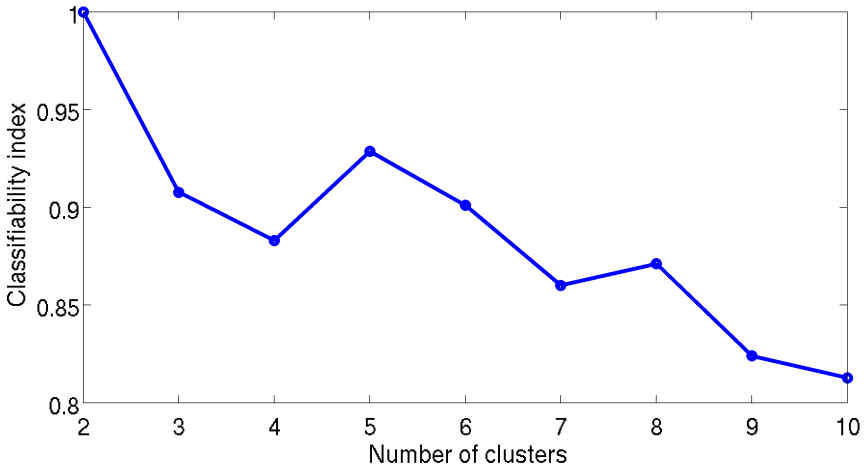

FIGURE 7.19 – Classifiability Index (CI) on WRF2.2 simulation output 2008-2014 warm season days

The four weather regimes obtained are represented on Figures 7.20 and 7.21. Table 7.4 shows the distribution of these four weather regimes in the 1086 days of the model output. It can be noticed that there is quite a good agreement between these regimes and the previous ones in terms of wind direction close to New Caledonia. There is indeed an easterly, a southerly, a trade wind and a northerly regime. Table 7.5 shows a comparison of the mean wind angles between the regimes determined with Blended Sea Winds and the regimes determined with the model, which enables to quantify the proximity between the regimes determined in the two different datasets. Apart from the easterly regime, the difference between the mean wind directions is less than 5°. The weather regimes in the model outputs

can therefore be used to make physical interpretations of the impact of the "real-world" synotpic circulation regimes observed with Blended Sea Winds.

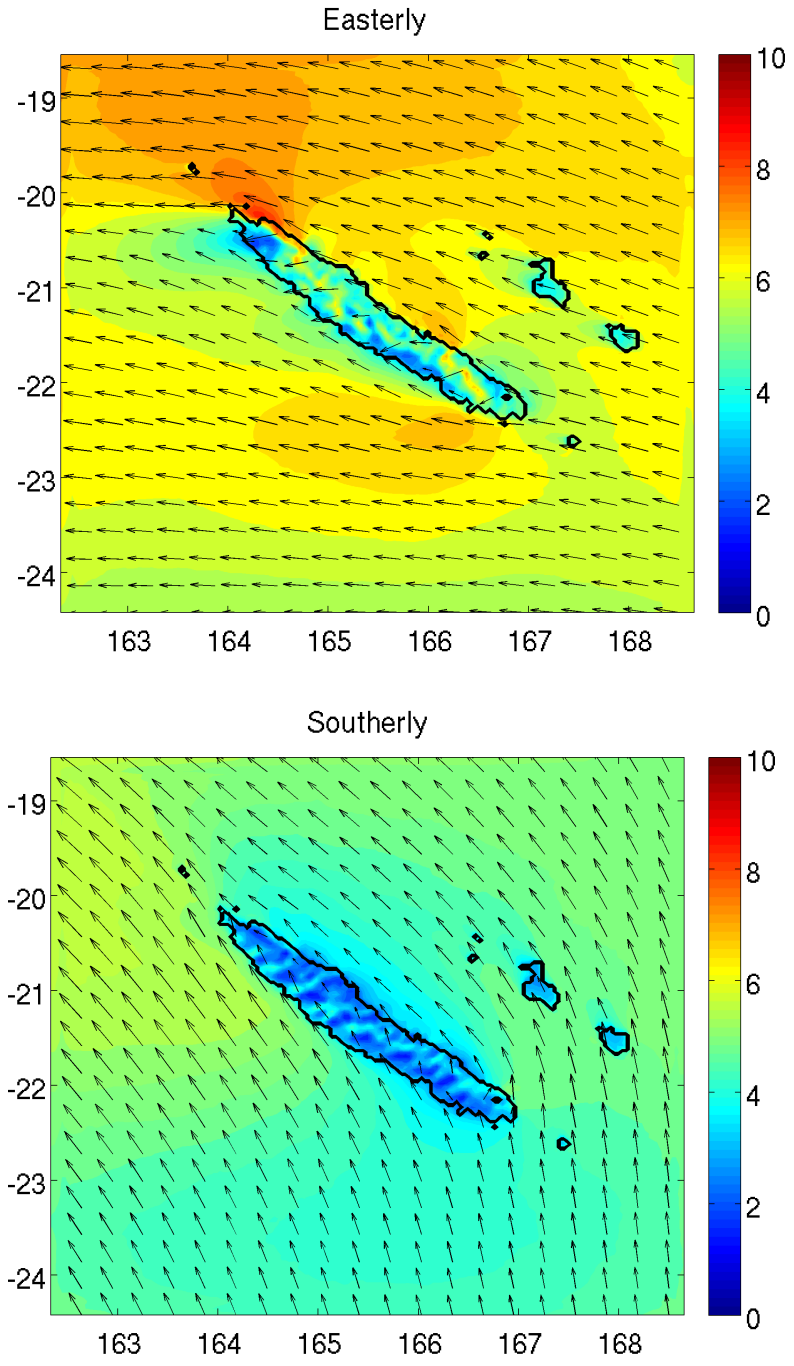

FIGURE 7.20 – Composites of 10-m wind (arrows) and associated wind speed (m/s, filled contours) in WRF2.2 simulation output for easterly and southerly regimes

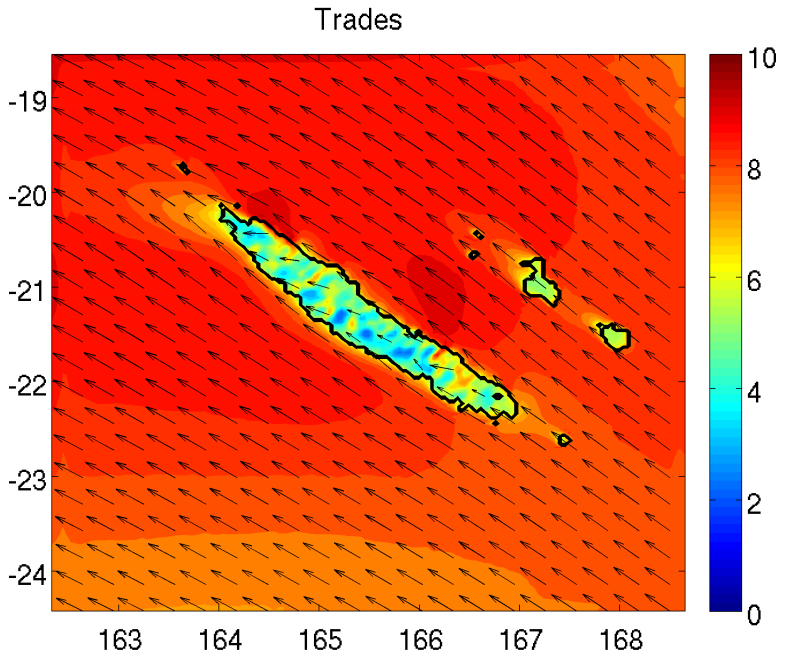

(a)

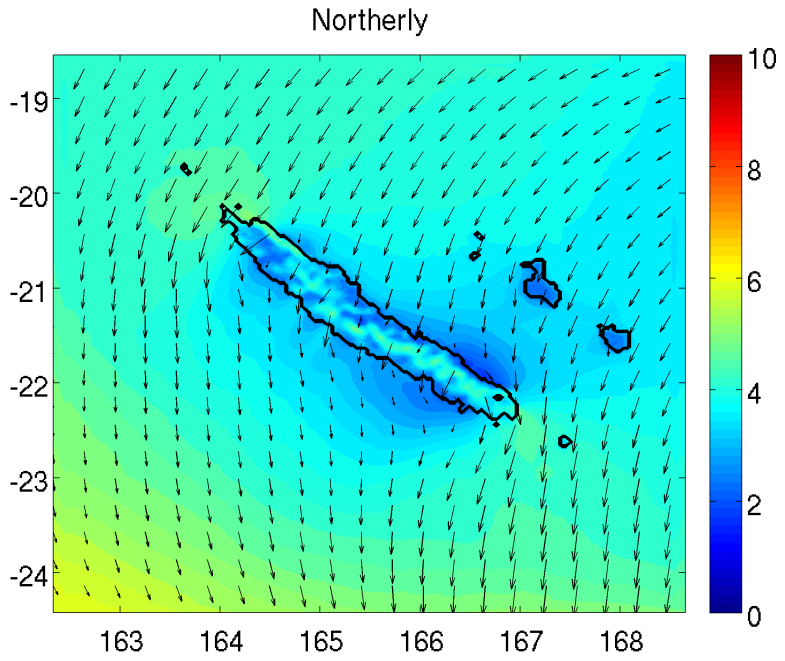

(b)

FIGURE 7.21 – Same as Figure 7.21 for trade and northerly regimes

Regime	Easterly	Southerly	Trades	Northerly	**Total**
Number	319	222	432	113	1086

TABLE 7.4 – Distribution of the warm season days 2008-2014 between the four weather regimes in WRF2.2 simulation output

Regime	Easterly	Southerly	Trades	Northerly
Blended Sea Winds	175.8	122.2	150.6	-107.1
WRF2.2	166.7	119.3	145.7	-103.2

TABLE 7.5 – Comparison between the mean wind angles (in °) in the box 161°E-170°E and 25°S-17°S between the Blended Sea Winds and the WRF2.2 weather regimes

7.2 Spatial classification of the Mainland model grid points

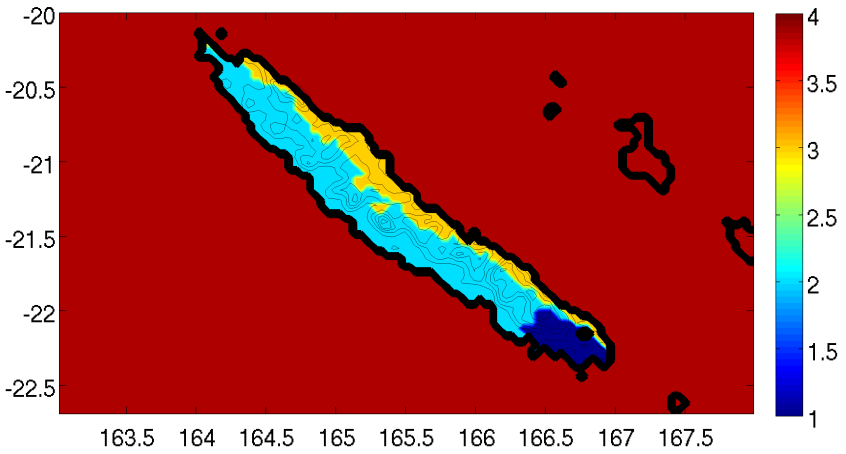

FIGURE 7.22 – Classification of the Mainland grid points in 3 clusters. The color represents the index number of the cluster.

Similarly to what has been done in Section 5.1, we are also able to perform an Ascendant Hierarchical Clustering of all the grid points in the simulation. We use a mask of the Mainland to exclude all the other points, and the four composite diurnal cycles of precipitation for each regime are concatenated at each point after being filtered by conserving only their three first harmonics. For the convenience of geographical interpretation, we are only able to retain three zones that appear in Figure 7.22. These zones match quite well with the ones that appear in Figure 5.14, with a neat separation between the West and East coast as well as a differentiation of the South. However, the clustering algorithm fails to isolate the mountain range, which might be blamed on the fact orography is smoothed in the model compared to reality.

7.3 Average rainfall and diurnal cycle for each weather type

The composite diurnal cycles averaged over all the Mainland points are represented for each weather regime in Figure 7.23. The model reproduces the expected average diurnal cycle peaking around 03 :00 PM. The northerly regime remains by far the wettest, but the hierarchy is somewhat modified for the other ones, with the trade regime being slightly wetter than the other two (southerly and easterly) that exhibit similar cycles. Another important point is the negative bias in the model that makes it underestimate the amount of rainfall falling over the Mainland by 2 to 3 mm per day if we compare the average cycles in Figures 6.15 and 7.23.

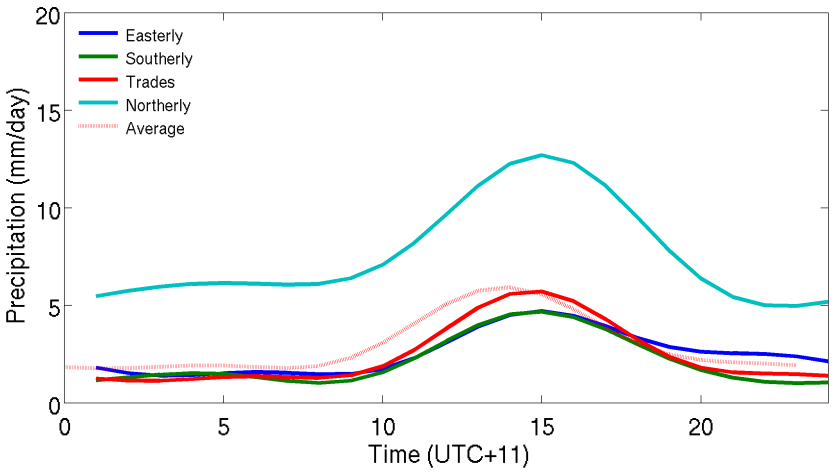

FIGURE 7.23 – Average diurnal cycle of precipitation (mm/day) in WRF2.2 simulation output on the Mainland for each weather type

7.4 Average rainfall and diurnal cycle for each spatial cluster

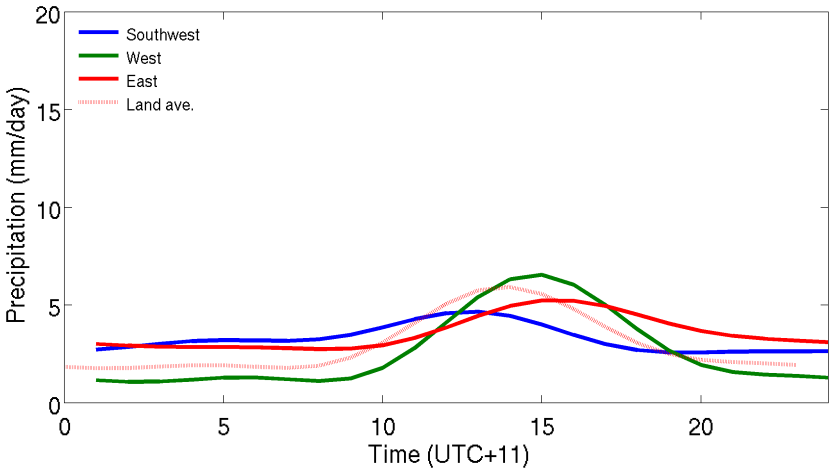

FIGURE 7.24 – Diurnal cycles of precipitations (mm/day) in WRF2.2 simulation output averaged on each geographical zone

Figure 7.24 illustrates the average rainfall cycle for each cluster in the model output. While the west coast (that includes the mountain range) shows a behavior that is quite similar to the one we saw with the rain gauge stations in Figure 6.17 (a sharp diurnal peak in the afternoon), the east exhibits a different pattern : the model fails to reproduce the non-standard East coast diurnal cycle and recreates a standard one instead. The average daily precipitation is quite similar for both zones, but the diurnal variations differ : the East coast has a higher minimum and smoother peak, whereas the West coast has very low minimum precipitation and a bigger peak. As for the southern zone, it cannot really be compared to the one of the rain gauge stations since it encompasses a partly different domain, but it is noteworthy to see that its average daily precipitation is quite similar to that of the two other zones. In other words, we do not have a neat driest or wettest zone as in the stations, and the domains are mostly determined by the pattern of their diurnal variability.

7.5 Geographical impact of each weather type

Here we choose to focus only on the comparison between the Western zone and the Eastern band, given that the Southern zone has very variable diurnal cycles depending on the synoptic winds. In Figure 7.25, the rainfall cycle on the West coast has a constant pattern and the regimes only influence the average precipitation and diurnal amplitude. The hierarchy of the regimes is similar to that in Figure 7.24, with the southerly regime the driest.

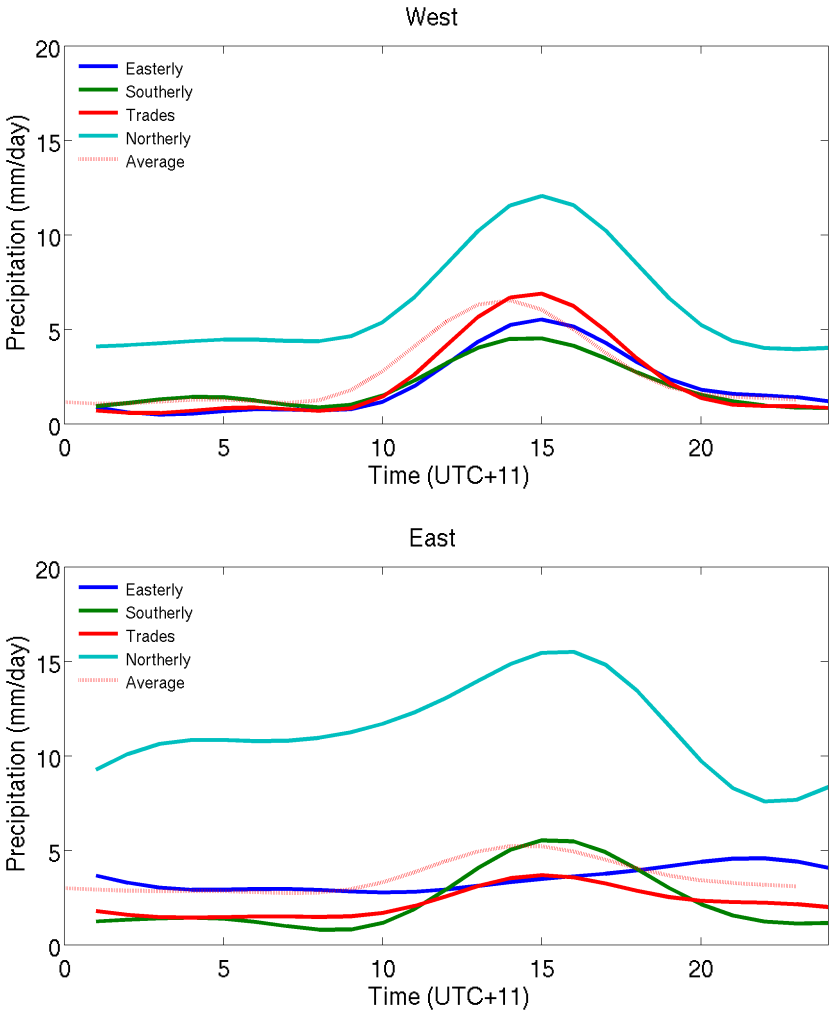

FIGURE 7.25 – Diurnal cycles of precipitation (mm/day) in WRF2.2 simulation output for each weather regime on the East and West coasts

As for the East coast, we fortunately find out that it has a more specific variability although it did not seem very evident in the average. The northerly and easterly regimes are characterized by non-standard diurnal cycles, while the southerly regime entails a standard diurnal cycle alike the one we noticed in the rain gauge stations. Only the trade regime cycle does not match observations since it is standard in the model and non-standard in rain gauge stations. Given that the majority of days are in trade regime in the model outputs (see Table 7.4), the fact that the average diurnal cycle of the East coast has a wrong pattern in the model is due to a bias the trade regime cycle. Indeed, the trade regime has a critical orientation between easterly and southerly : depending on its angle, it may either hit the Mainland by the East (like the easterly regime) or the West coast (like the southerly regime). Then, the East coast may either be on the windward or leeward side, which will change its diurnal cycle of rainfall.

Regime	South	West	East
Easterly	0.72	2.34	0.52
Southerly	0.98	1.98	2.02
Trades	0.73	2.71	0.98
Northerly	1.44	1.38	0.75

TABLE 7.6 – Ratios of the diurnal amplitude by the mean daily precipitation in the WRF 2.2 output

Nevertheless, even if it does not exhibit the expected average diurnal cycle on the East coast, the model can still be used to study the particular impact of the southerly wind regime, when the East coast is on the leeward side. Table 7.6 gathers for each regime and each geographical zone the values of the ratio of the diurnal amplitude by the mean daily precipitation. The amplitude is defined as the difference between the daily minimum and maximum. A higher ratio is synonymous of more intense diurnal variability relative to the mean, even though the average daily precipitation in itself is not so high. The fact is that on the East coast, the southerly regime is characterized by a ratio that is more than twice higher as the other regimes, with a value of 2.02. It is even one of the highest ratios, and the other ones can be found out on the West coast that usually exhibits a strong standard diurnal cycle. Table 7.7 shows the same ratios for the observations in the rain gauge stations. For the East coast cluster, the southerly regime also shows a ratio (1.34) that is roughly twice as big as those of the other regimes. Therefore, it is still possible to say that even in the model, the southerly regime is responsible for a very strong diurnal cycle on the East coast similar to that of the observations. The mechanisms for this behavior are being investigated in the next chapter.

Regime	Range	Northwest	Southwest	East
Easterly	1.56	2.05	1.16	0.66
Southerly	1.53	0.86	0.69	1.34
Trades	1.65	2.55	0.58	0.83
Northerly	1.31	1.40	0.93	0.39

TABLE 7.7 – Ratios of the diurnal amplitude by the mean daily precipitation in the rain gauge observations

Changing synoptic wind patterns and impacts on the diurnal cycle in the simulation

8.1 Preliminary note on diurnal cycle representation

The following sections will feature diurnal cycle representations as distance-time Hovmöller diagrams. This figures were generated thanks to a regridding of the original data on a grid that has been rotated by 45°, so that its longer axis coincides with the axis of the Mainland (see Figure 8.26). The regridding interpolation method is a nearest-neighbor interpolation provided by the MATLAB griddata function. The distance coordinate that appears in the next Hovmöller diagrams is the distance on the x-axis (cross-shore distance) at the y-coordinate where the Mainland is the widest. Distances were computed from the new grid coordinates using a Mercator projection. The Hovmöller diagrams therefore represent the diurnal evolution of the parameters along the width of the Mainland after averaging along its length.

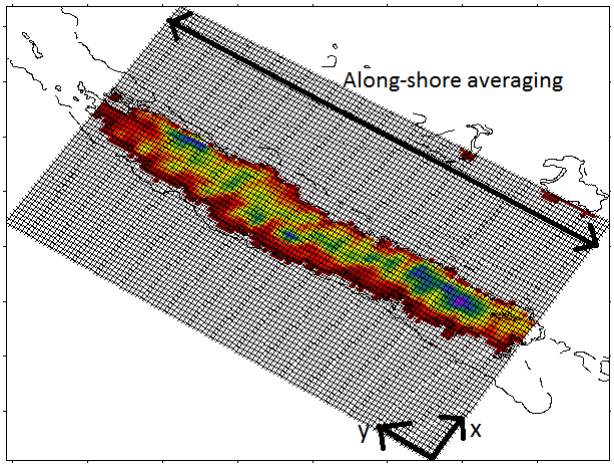

FIGURE 8.26 – New grid rotated by 45° in the axis of the Mainland

8.2 General features of the diurnal cycle

In terms of land-sea breeze, one of the most striking fact in the New Caledonian diurnal cycle is the stark contrast between the East and West coast. On average, while the West coast experiences a strong sustained cycle with land breeze at the end of the night and sea breeze in the afternoon, the East coast shows very little diurnal wind variability. This is illustrated by Figure 8.27 which shows the diurnal wind anomalies (values of the wind components at a given time minus average value for the composite day) and the associated speed for two periods : 06 :00 to 09 :00 AM and 14 :00 to 17 :00

PM, averaged over warm season days in the model simulation.

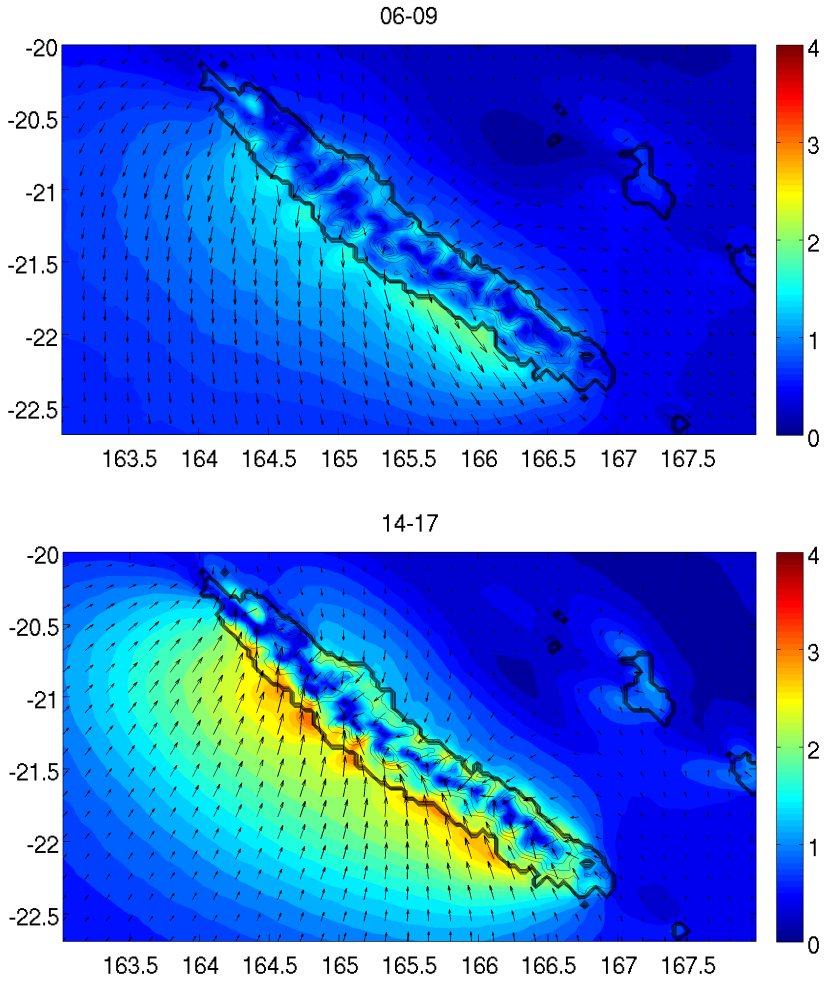

FIGURE 8.27 – Average diurnal wind anomalies (instantaneous wind minus daily average, arrows) and norm of the anomalies (filled contours, m/s) in the time intervals 06-09 AM and 14-17 PM

The intensity of the land breeze in the morning and the intensity of the sea breeze in the afternoon are indeed up to 4 times higher in the West than in the East. This can be accounted for with orographic differences. As we mentioned in the Introduction, on the East coast, the mountain slopes are steeper and stand closer to the sea. On the West coast, and especially in the central West coast, there are large flat plains. Consequently, during the diurnal cycle of solar radiation, the plains on the West coast heat up more than the mountain flanks of the East coast, and the air above the ground gets warmer on the West coast too. This can be deduced from the Hovmöller diagram in Figure 8.28 where higher sensible heat fluxes can be noted on the western side during the period of insolation. The horizontal pressure gradient above surface between land and sea is therefore stronger on the West coast, and so is the land-sea breeze system. Actually, it will be considered that there is approximately no sea breeze on the East coast in average conditions.

However, this does not mean that rainfall does not occur on the East coast, far from it. If we consider the diurnal cycle of total precipitable water in the atmosphere, shown in Figure 8.28, we notice that whatever the moment, this quantity is always higher to the East. This can be accounted for the fact that in most cases, the East coast is on the windward side of New Caledonia and moisture tends to accumulate there owing to the steep orography. Favorable conditions for precipitation are therefore

present most of the time, which would explain why on average the East coast is rainier but with little diurnal variability.

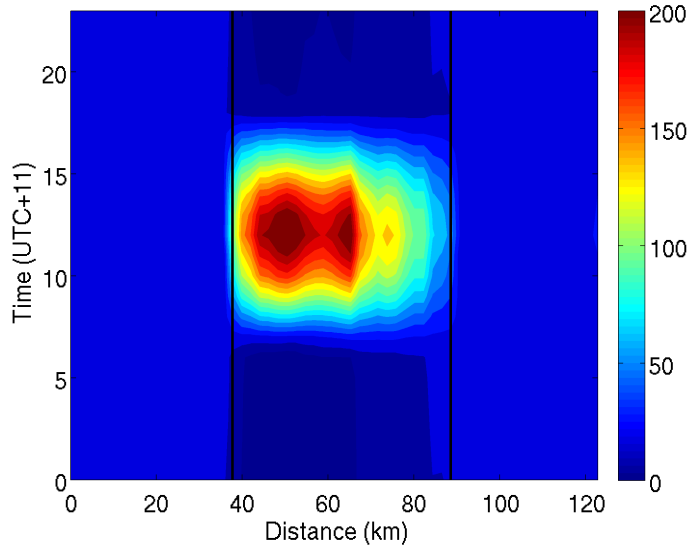

(a)

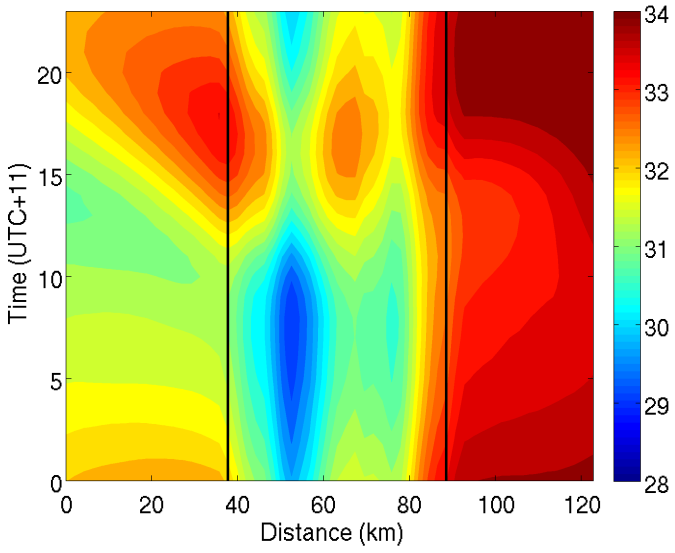

(b)

FIGURE 8.28 – Hovmöller diagram of the diurnal cycle after averaging on the length of the rotated grid (a) Sensible heat fluxes (W/m^2) (b) Total precipitable water (kg/m^2) in the atmosphere considered as a single layer. The vertical bars roughly represent the western and eastern limits of the Mainland.

8.3 Comparison of the easterly and southerly regimes

Figure 7.25b suggests that although the model fails to represent the average non-standard diurnal cycle on the East coast, it does quite well in the case of the easterly regime (for which the cycle is rather flat) and the southerly regime (for which the cycle is abnormally standard). This is why it is still possible to analyze the underlying mechanisms of the diurnal cycle that we observed before in the case of these two regimes.

8.3.1 Diurnal variability of the wind

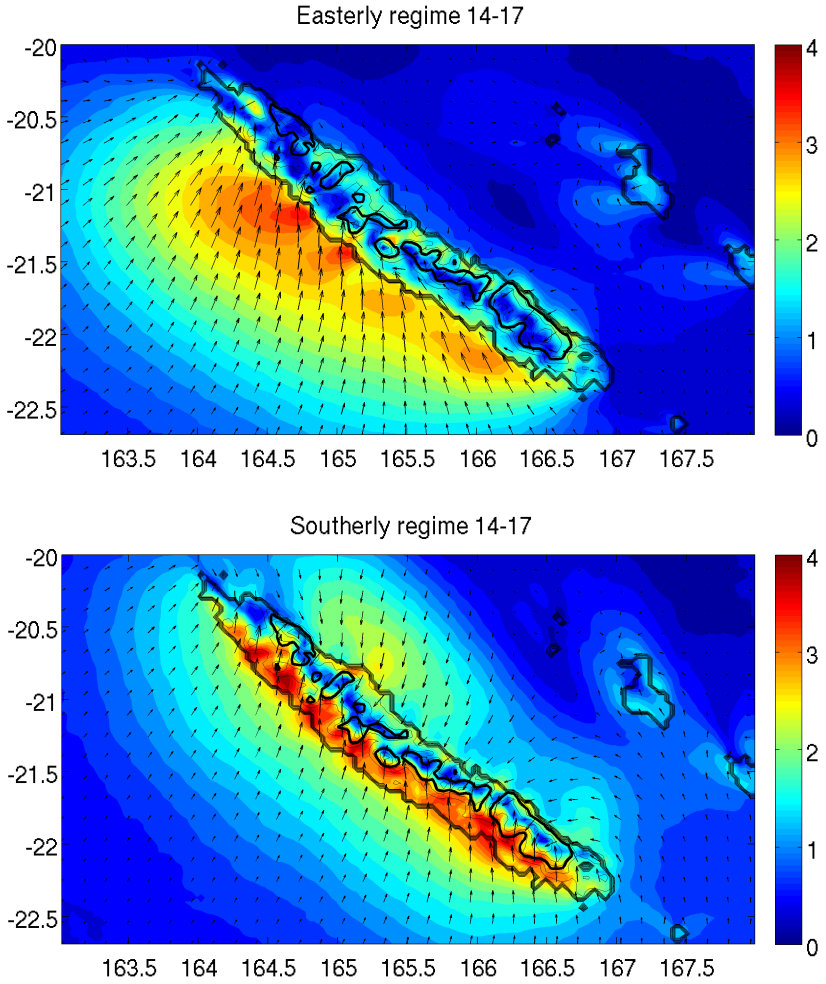

FIGURE 8.29 – Average diurnal wind anomalies (instantaneous wind minus daily average, arrows) and norm of the anomalies (filled contours, m/s) for the 14-17 time interval in easterly and southerly regimes. Bold contour represents the 400 m height.

Figure 8.29 highlights the comparison between the sea breezes for both regimes and enables to notice that in the southerly regime, a sea-breeze like circulation appears on the East coast too while it does not exist neither in the easterly regime nor in the average wind field anomalies in Figure 8.27. In the meantime, the diurnal anomalies on the West coast penetrate far more inland in southerly than in easterly regime.

8.3.2 Precipitation and moisture convergence variability

For each regime, the Hovmöller diagrams of the cycles of precipitation and low-level moisture convergence diurnal anomalies are represented on Figure 8.30. For both regimes, we notice a strong positive anomaly of precipitation over the Mainland between 12 :00 and 18 :00 that coincides with a positive anomaly of low-level moisture convergence. This diurnal cycle of precipitation anomalies is not surprising in itself since it corresponds to the diurnal peak that has been described several times before. This peak can therefore be related to a peak in moisture convergence that creates favorable conditions for the triggering of precipitations.

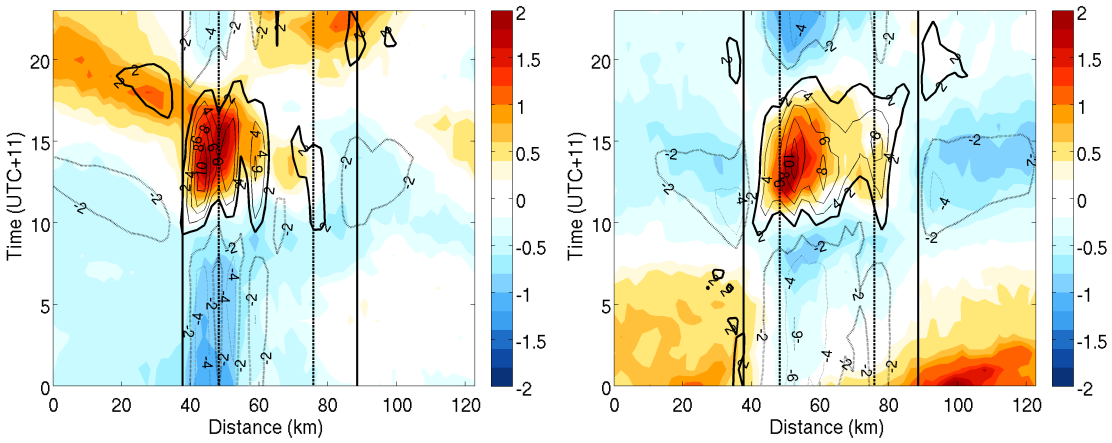

(a) (b)

FIGURE 8.30 – Hovmöller diagram of the diurnal precipitation anomalies (mm/day, filled contours) and moisture convergence anomalies (10^7 kg/kg/s, contours) in the layer between surface pressure and surface pressure minus 30 hPa (a) Easterly regime (b) Southerly regime. Dashed lines separate between West coast, East coast and middle zone (East or West depending on the y-coordinate)

The link between moisture convergence and precipitation has been extensively documented and moisture convergence is indeed often used as a good indicator for rainfall. Peixoto and Oort (1992) provide the formula for the atmospheric water balance :

$$P - E = -\frac{\partial W}{\partial t} - \nabla \cdot \mathcal{Q}$$

where

$$W = \frac{1}{g}\int_{p_s}^{p=0} q dp$$

is the total precipitable water in the atmospheric column defined as the integral of specific humidity, and

$$\mathcal{Q} = \frac{1}{g}\int_{p_s}^{p=0} q\vec{u} dp$$

is the integrated horizontal water vapor flux. Although the moisture convergence that is represented on Figure 8.30 only corresponds to humidity integrated between the surface pressure and the surface pressure minus 30 hPa (e.g 1000 hPa and 970 hPa), and not over all the atmospheric column, it can still be considered as a cause for precipitation given that much of the humidity is located in the lowest levels of the atmosphere. As a result, its diurnal cycle can be tightly related to the diurnal cycle of rainfall. A quick comparison between the two regimes shows that the afternoon positive anomalies of precipitation and moisture convergence are more concentrated to the west coast in the easterly regime, while they spread to the east coast in southerly regime. As a whole, these two diurnal cycles give the expected results compared to Figure 7.25, with a standard diurnal cycle of precipitation on the West in both regimes, while the East coast has a flat diurnal cycle in easterly regime and a standard cycle in southerly regime.

8.3.3 Cross-shore wind and moisture convergence variability

The variability of precipitation being linked to that of moisture convergence, it is therefore crucial to understand how moisture convergence diurnal variability is governed. Figure 8.31 superimposes the same contours of moisture convergence anomalies as in Figure 8.30, along with the diurnal anomalies of the cross-shore wind component, that is to say the x-component of the wind vectors in the rotated grid.

The cross-shore wind anomalies exhibit a strong diurnal cycle in the West, with a peak of westerly anomalies from the late morning to the late afternoon that represents the strong West coast sea breeze. This anomaly goes deeper into the Mainland in the case of the southerly regime than the easterly regime. In the same time interval, on the East coast, a weaker easterly wind anomaly can be noticed only in the case of the southerly regime, which corroborates the results in Figure 8.27. The place of strong moisture convergence tends to coincide with the maximum of westerly wind anomaly due to sea breeze. In southerly regime, the extension of the convergence zone to the east also coincides with the tip of the East coast sea-breeze-like anomaly.

Moreover, when we carry out a decomposition of specific humidity and wind vectors as the sum of their daily mean and the cycle of their diurnal anomalies, we are able to calculate separately the diurnal cycle of moisture convergence engendered by the diurnal cycle of winds and the diurnal cycle of moisture convergence engendered by the diurnal cycle of humidity (not shown). It appears that in the case of our synoptic regimes, moisture convergence diurnal variability is indeed governed by the diurnal variability of winds, and not by the diurnal variability of atmospheric humidity itself.

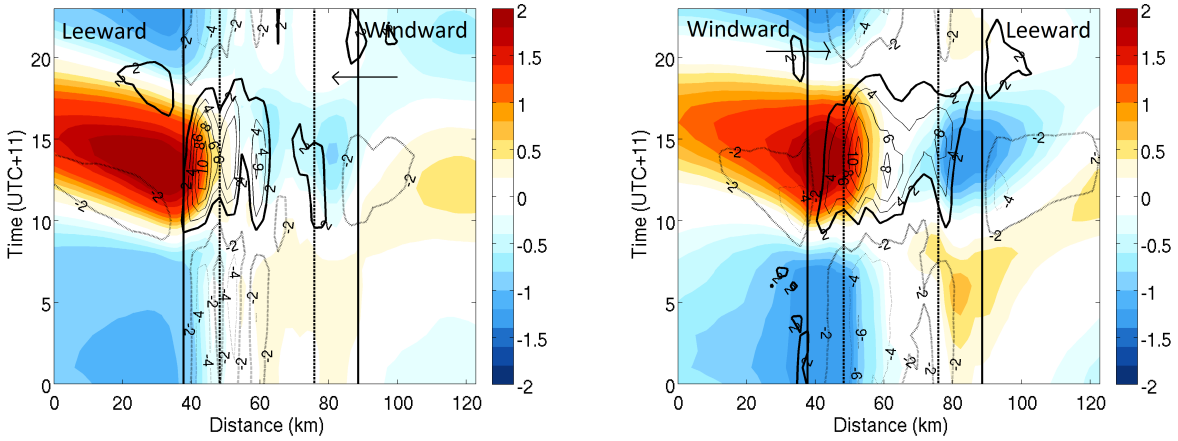

(a) (b)

FIGURE 8.31 – Hovmöller diagram of the diurnal cross-shore wind anomalies at 10 m (m/s, filled contours) and moisture convergence anomalies (10^7 kg/kg/s, contours) in the layer between surface pressure and surface pressure minus 30 hPa (a) Easterly regime (b) Southerly regime. Dashed lines separate between West coast, East coast and middle zone (East or West depending on the y-coordinate)

8.3.4 Impact of wind speed and orographic features

When comparing the easterly and southerly regimes in terms of wind variability, it is quite obvious to notice that the strong West coast sea breeze either goes against the synoptic winds (easterly regime) or in the same direction as them (southerly regime). This has an impact on the speed of the wind hitting the New Caledonian moutain range, and more precisely on its evolution during the day. Figure 8.32 illustrates the evolution of the total wind speed during the day on both sides of the island and for both regimes. A first point that needs to be mentioned and that could already be seen in Figures 7.20 and 7.21 is that the southerly regime is one of the slowest, along with the northerly regime. In Figure 8.32, the wind speed is indeed higher for the easterly regime. Moreover, while the easterly regime features a constant incoming wind speed on the windward coast (East coast), the southerly regime exhibits more diurnal variability on its own windward coast, the West coast. This diurnal variability with wind speed peaking at approximately 7 m/s only on the West coast in the afternoon is due to

the intensification of the dominant winds by the sea breeze that appears during this time interval.

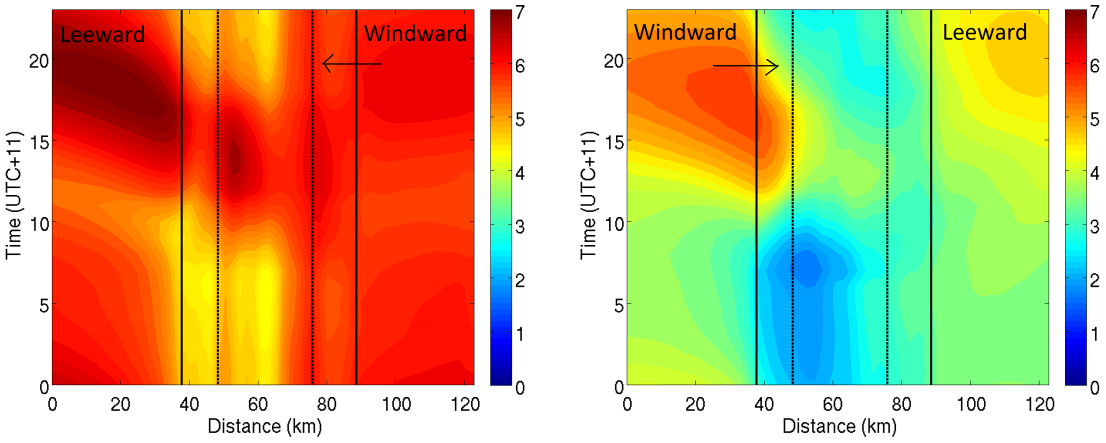

(a) (b)

FIGURE 8.32 – Hovmöller diagram of the total wind speed at 10 m (m/s) (a) Easterly regime (b) Southerly regime. Dashed lines separate between West coast, East coast and middle zone (East or West depending on the y-coordinate)

The question of wind speed is crucial when dealing with the interaction of orography and winds. The main question when a wind flow hits a mountain is indeed to know whether it will be blocked and split around or go over it. This has been extensively documented in multiple configurations, with the help of linear theory for orographic flows. This theory provides a few dimensionless parameters that enable to understand the behavior of the flow. One of these parameters is the orographic Froude number, defined as the ratio $Fr = \frac{U}{Nh}$ where U is the speed of the incoming flow, N is the Brünt-Vaisala frequency representing the static stability of the air column and h is the height of the obstacle (Houze, 2012). This parameter has been widely used, for instance by Smith (1988), Overland and Bond (1993) or Lefèvre et al. (2010). It can be seen as the ratio between the theoretical height $\frac{U}{N}$ the air parcel can reach owing to its oscillations in the air column while it is moving horizontally, and the height of the obstacle. According to Smith (1988) and Houze (2012), it is generally accepted that the flow is blocked for $Fr < 1$ and that it can go over the obstacle for $Fr > 1$.

In the case of our New Caledonia model, if we take the mean of the maximum heights (see Figure 2.6) at each latitude band that comprises a part of the range (between 22.2°S and 20.5°S), we find a value of 622 m. Then, we can consider an order of magnitude of the height of the obstacle of $h = 600$ m. The real value of the average height of the range is closer to 800 m but it is reasonable to keep a value of 600 m when considering model data because the model considers a lower mountain range due to orography smoothing.

As the vertical profiles of the Brünt-Vaisala frequency N are plotted at various times of the day (not shown), it can be noticed that the values of N remain around $10^{-2}s^{-1}$ in the first 1000 m in the course of the day. This is consistent with the order of magnitude of N ($N \sim 10^{-2}s^{-1}$) for a typical atmospheric stratification (Overland and Bond, 1993; Lefèvre et al., 2010), and it can be considered constant over the length of the day. As for U, it varies in the course of the day, especially in Southerly regime under the influence of the West coast sea breeze. The value we take for U is the maximum wind speed in the windward region of the rotated grid.

Figure 8.33 represents the diurnal cycle of Froude number. While it remains almost constant and

greater than 1 in the course of the day for the easterly regime, it starts with values less than 1 before peaking with values greater than 1 in the afternoon for the southerly regime. In other words, it seems that in easterly regime, the flow is always fast enough to go over the moutain ridge while in southerly regime, the flow is blocked at the beginning of the day and needs an intensification with sea breeze to go over the mountain. This is in good agreement with what has already been observed in Figure 8.29 : the afternoon diurnal wind anomalies (sea breeze) on the West coast penetrate inland in southerly regime while it stops at the shore in easterly regime.

Of course, this computation in order of magnitude is very sensitive to the values taken for U and h : lower values of U or higher values of h might give a Froude number that is always less than 1 in southerly regime, but the contrast between the two regimes for their diurnal cycles of Froude number would remain and this supports the fact that the interaction between the flow and orography will change in the course of the day for the southerly but not for the easterly regime.

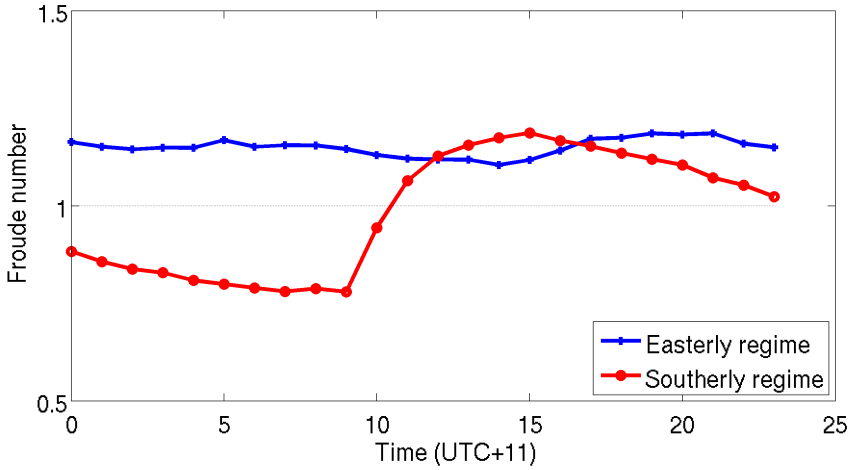

FIGURE 8.33 – Diurnal cycle of Froude number $Fr = \frac{U}{Nh}$ in easterly and southerly regime for $N = 10^{-2}$ s^{-1} and $h = 600$ m

8.3.5 A proposed explanation for the different diurnal cycles of precipitation

In all regimes, due to the diurnal cycle of sea breeze and orographic effects, moisture convergence peaks over the mountain range in the middle of the island. In the easterly regime, moisture accumulates all over the day on the East coast (windward side) due to orographic lifting and condensation : the East coast is rainy with little diurnal variability. In parallel, intense afternoon sea breeze on the West coast creates moisture convergence over the range and the West coast plains. This convergence is strong owing to the fact sea breeze opposes synoptic winds. Rainfall reaches a maximum on the West coast in mid-afternoon, before decreasing as moisture convergence decreases with the disappearing of the sea breeze : this gives the standard diurnal cycle on the West coast.

In the southerly regime, contrary to the easterly regime, there is little moisture on the East coast at the beginning of the day because the East coast is on the leeward side. Moreover, the flow is blocked and split when it arrives on the island because the speed is too weak. In the afternoon, the wind speed intensifies thanks to sea breeze, the flow is able to pass over the mountains. While going over the obstacle, it gets slowed down (as shown by the easterly wind anomaly that we can observe on Figure 8.30) : this creates wind and moisture convergence on the leeward East coast (hence the extension of the moisture convergence zone compared to the easterly regime), a condition that is favorable for precipitation. Precipitation peaks in the afternoon, but decreases in the same time as moisture convergence

and incoming wind intensity when the West coast sea breeze weakens. Therefore, it can be said that in southerly regime, the diurnal cycle of precipitation on the East coast correlates with the diurnal cycle of sea breeze of the West coast.

Conclusions

New Caledonia exhibits a strong temporal and spatial variability in terms of diurnal rainfall patterns. Temporal variability is conditioned by the synoptic circulation around the island, which is itself strongly influenced by large-scale modes of variability such as the Madden-Julian oscillation, especially in warm season. Although it is difficult to put forward a direct impact of the MJO on the diurnal precipitations over New Caledonia most of the time, an indirect effect of the MJO on New Caledonian weather regimes can be highlighted statistically and is consistent with existing theories on the effects of positive equatorial convective anomalies on tropical and subtropical atmospheric circulation : the eastward propagation of the MJO is likely to generate more easterly winds over New Caledonia first, followed by more northerly winds bringing a lot of moisture and rainfall when the convective patch reaches the Western Pacific, and followed again by more southerly winds at the end of the MJO cycle. At a smaller spatial scale, the influence of the direction of synoptic winds on the diurnal cycle of rainfall is related to two aspects : the average moisture that is brought by the synoptic winds on the one hand, and the relative orientation between the synoptic winds and the West coast sea breeze system on the other hand. As a rule, most areas of the Mainland feature a standard diurnal cycle with an afternoon rainfall peak around 03 :00 PM, preceded and followed by little precipitation. This diurnal cycle is associated to processes occurring mostly over the mountain range in the time interval of strongest western sea breeze. However, the East coast has an altogether different cycle with less variability but more rain than the West coast, owing to several particularities among which its location on the windward side for most regimes, and the steep mountain slopes located close to the sea. This behavior can nonetheless be modulated in case of a particular orientation of the winds like in the southerly regime : the East coast is wind-shadowed for a part of the day and gets swept by the wind thanks to the West coast sea breeze, which tends to correlate its diurnal cycle of precipitation with the diurnal cycle of sea breeze on the other side of the mountains.

The first insight of the diurnal cycle of precipitation over New Caledonia presented in this work calls for more investigations in several directions. First of all, as far as the geographical classification of rainfall is concerned, putting into perspective a bigger quantity of data with several independent observational datasets (rain gauge stations, satellite data, radar) would bring additional certainties on the spatial distribution of precipitation. In another direction, the interaction between synoptic circulation, mesoscale wind effects like the sea breeze and precipitation could be studied more extensively by resorting to idealized model simulations for which the synoptic wind direction would be prescribed. Getting inspiration from what has been done in other studies about islands in Hawaii (Nguyen et al., 2010; Carlis et al., 2010), this study should also include sensitivity tests by modifying some model parameters like the orography (with no mountain, with higher or lower mountain) or thermal and diabatic effects, that probably play a role in the moisture convergence or in the development of sea breezes. Finally, it would also be relevant to carry out other complete model simulations, like the one used in this study, with more recent models, such as WRF version 3.7 or Météo France AROME. These models provide supplementary diagnostic terms, such as the humidity tendencies due to thermal, turbulent or convective effects, that will enable further analysis of the underlying physical processes of rainfall.

Appendix 1 : list of rain gauge stations

Station	Start date	End date	Longitude (°E)	Latitude (°S)	Altitude (m)
Bouraké	2000/12/13	2014/12/31	165.9998	21.9425	53
Nassirah	1999/09/13	2014/12/31	166.0632	21.815	52
Bourail	1997/06/11	2014/12/31	165.4938	21.5548	25
Nessadiou	1991/05/01	2014/12/31	165.4802	21.6205	2
Me Para	1991/07/01	2014/12/31	165.5812	21.4742	835
Canala	1993/06/15	2014/12/30	165.9692	21.5263	35
Dumbéa	1998/02/04	2014/12/31	166.4808	22.1357	14
Hienghène	1994/02/01	2014/12/31	164.9495	20.6883	22
Houaïlou	1993/01/01	2014/12/31	165.628	21.2783	11
Col des Roussettes	1999/06/01	2014/12/31	165.454	21.4233	361
Oueholle	1996/07/11	2008/12/01	164.525	20.588	155
Koné	1995/07/01	2014/12/31	164.8335	21.0513	9
Tango	1998/03/01	2014/12/31	165.0262	20.9837	341
Koumac	1993/11/15	2014/12/31	164.2842	20.5587	25
La Foa	1995/12/15	2014/12/31	165.8147	21.7013	12
Nouméa	1996/01/01	2014/12/31	165.4528	22.276	70
Phare Amédée	1991/01/01	2014/12/31	166.4673	22.4783	3
La Tontouta	1996/01/01	2014/12/31	166.2223	22.0173	37
Poindimié	1993/01/01	31/12/2014 2014/12/31	165.328	20.9325	14
Aoupinié	1991/01/01	2014/12/31	165.2853	21.177	905
Pouébo	1992/05/01	2011/06/06	164.587	20.3982	13
Pouembout	1992/04/03	2009/02/19	164.9013	21.1195	27
Poya	1999/06/01	2014/12/31	165.157	21.3453	7
Népoui	1990/04/01	2014/12/31	165.0022	21.3182	82
Borindi	1992/01/08	2014/12/31	166.4915	21.7963	5
Touho	1993/01/01	2014/12/31	165.2545	20.7893	2
Yaté Mrié	1993/01/01	2014/12/31	166.939	22.1565	25
Montagne des Sources	1991/01/01	2014/12/31	166.5932	22.1438	773
Rivière Blanche	2000/12/06	31/12/2014 2014/12/31	166.7263	22.1327	171

Table 8.8 – List of Météo France rain gauge stations and coordinates

Appendix 2 : influence of MJO in rain gauge precipitation

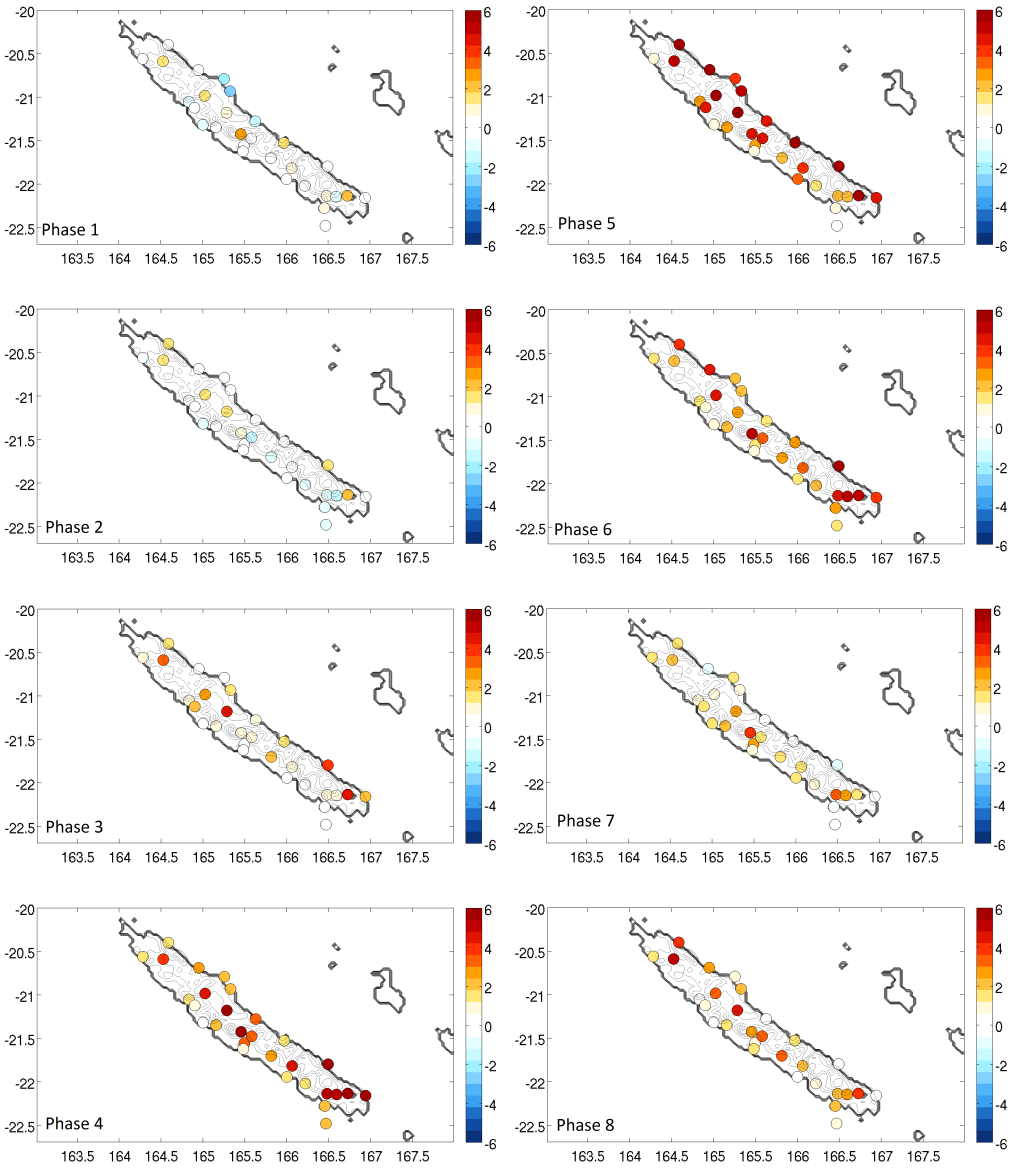

FIGURE 8.34 – Mean precipitation anomalies (mm/day) between the MJO phase composite and the warm season climatological mean in Météo France 1991-2014 data

Appendix 3 : influence of MJO in TRMM precipitation

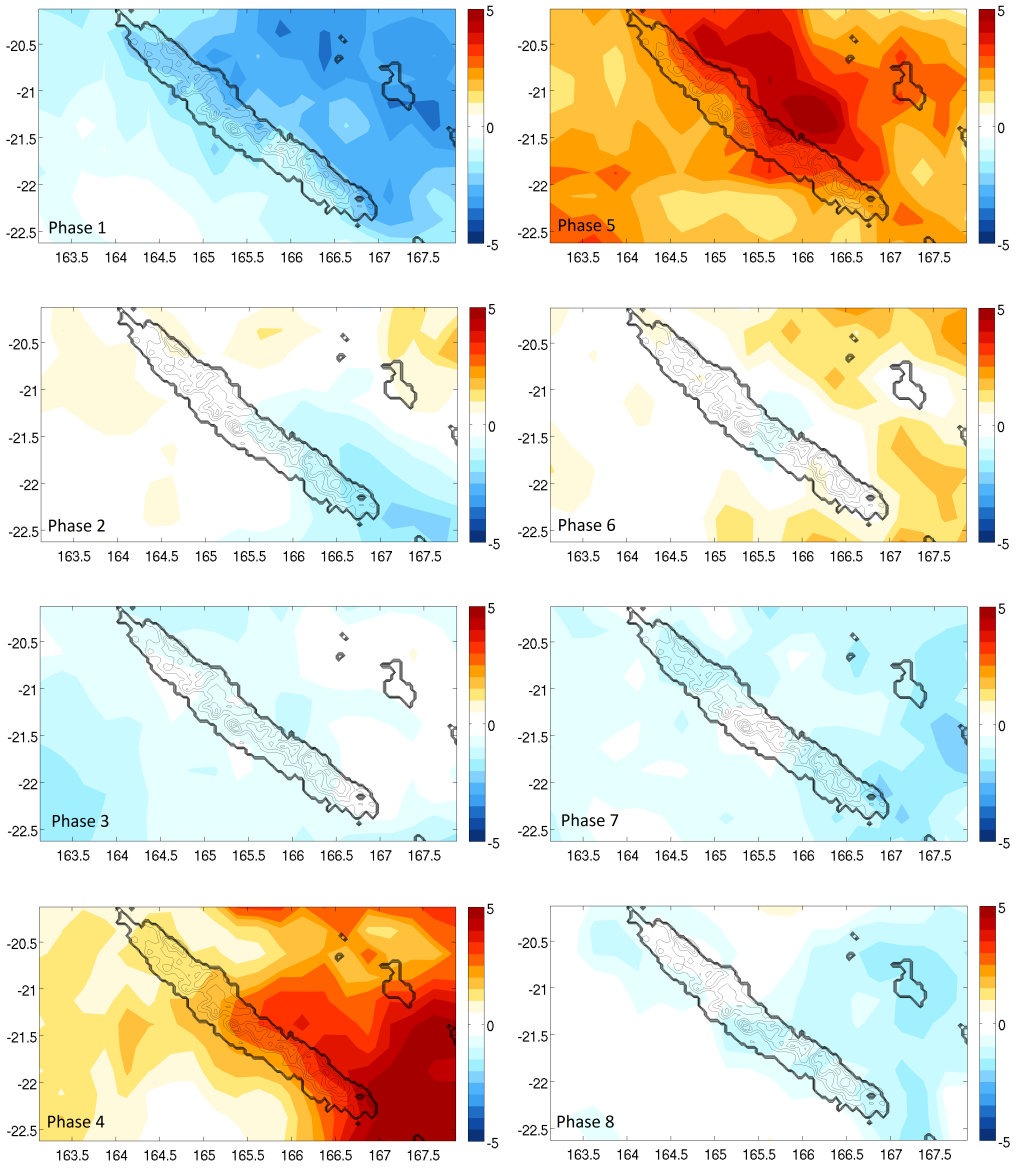

FIGURE 8.35 – Mean precipitation anomalies (mm/day) between the MJO phase composite and the warm season climatological mean in TRMM 1998-2014 satellite data

References

R. Barbero and V. Moron. Seasonal to decadal modulation of the impact of El Niño-Southern Oscillation on New Caledonia (SW Pacific) rainfall (1950-2010). *Journal of Geophysical Research*, 116, 2011.

D.N. Carlis, Y-L. Chen, and V.R. Morris. Numerical Simulations of Island-Scale Airflow over Maui and the Maui Vortex under Summer Trade Wind Conditions. *Monthly Weather Review*, 138 :2706–2736, 2010.

T.W. Cronin, K.A. Emanuel, and P. Molnar. Island precipitation enhancement and the diurnal cycle in radiative-convective equilibrium. *Quarterly Journal of Royal Meteorological Society*, 141 :1017–1034, 2015.

A.E. Gill. Some simple solutions for heat-induced tropical circulation. *Quarterly Journal of Royal Meteorological Society*, 106 :447–462, 1980.

R. Hidayat and S. Kizu. Influence of the Madden-Julian Oscillation on Indonesian rainfall variability in austral summer. *International Journal of Climatology*, 30 :1816–1825, 2010.

R.A. Houze. Orographic effects on precipitating clouds. *Reviews of Geophysics*, 50, 2012.

M. Kanamitsu, W. Ebisuzaki, J. Woollen, S-K. Yang, J-J. Hnilo, M. Fiorino, and G.L. Potter. NCEP-DOE AMIP-II Reanalysis (R-2). 2002.

J. Lefèvre, P. Marchesiello, N.C. Jourdain, C.E. Menkes, and A. Leroy. Weather regimes and orographic circulation around New Caledonia. *Marine Pollution Bulletin*, 61 :413–431, 2010.

L.B. Leopold. The interaction of trade wind and sea breeze, Hawaii. *Journal of Meteorology*, 6 : 312–320, 1949.

A. Leroy. Utilisation des Prévisions Saisonnières en Nouvelle-Calédonie. Technical report, 2006. Note de la DP n ° 6.

B.S. Love, A.J. Matthews, and G.M.S. Lister. The diurnal cycle of precipitation over the Maritime Continent in a high-resolution atmospheric model. *Quarterly Journal of Royal Meteorological Society*, 137 :934–947, 2011.

R.A. Madden and P.R. Julian. Detection of a 40-50 Day Oscillation in the Zonal Wind in the Tropical Pacific. *Journal of the Atmospheric Sciences*, 28, 1971.

P-A. Michelangeli, R. Vautard, and B. Legras. Weather Regimes : Recurrence and Quasi-Stationarity. *Journal of the Atmospheric Sciences*, 52 :1237–1256, 1995.

V. Moron, R. Barbero, and A.W. Robertson. Subseasonal-to-interannual variability of rainfall over New Caledonia (SW pacific). *Climate Dynamics*, 2015a.

V. Moron, A.W. Robertson, J-H. Qian, and M. Ghil. Weather types across the Maritime Continent : from the diurnal cycle to interannual variations. *Frontiers in Environmental Science*, 2, 2015b.

HV Nguyen, Chen Y-L., and F. Fujioka. Numerical Simulations of Island Effects on Airflow and Weather during the Summer over the Island of Oahu. *Monthly Weather Review*, 138 :2253–2280, 2010.

J.E. Overland and N. Bond. The Influence of Coastal Orography : The Yakutat Storm. *Monthly Weather Review*, 121 :1388–1397, 1993.

S.C. Peatman, A.J. Matthews, and D.P. Stevens. Propagation of the Madden-Julian Oscillation through the Maritime Continent and scale interaction with the diurnal cycle of precipitation. *Quarterly Journal of Royal Meteorological Society*, 140 :814–825, 2014.

J.P. Peixoto and A.H. Oort. *Physics of Climate*. Springer, 1992.

J-H. Qian. Why Precipitation Is Mostly Concentrated over Islands in the Maritime Continent. *Journal of the Atmospheric Sciences*, 65 :1428–1440, 2008.

J-H. Qian, A.W. Robertson, and V. Moron. Diurnal Cycle in Different Weather Regimes and Rainfall Variability over Borneo Associated with ENSO. *Journal of Climate*, 26 :1772–1790, 2013.

H. Rui and B. Wang. Development Characteristics and Dynamic Structure of Tropical Intraseasonal Convection Anomalies. *Journal of the Atmospheric Sciences*, 47 :357–379, 1990.

R.B. Smith. Linear Theory of Stratified Flow past an Isolated Mountain in Isosteric Coordinates. *Journal of the Atmospheric Sciences*, 45 :3889–3896, 1988.

A.H. Sobel, C.D. Burleyson, and S.E. Yuter. Rain on small tropical islands. *Journal of Geophysical Research Letters*, 116, 2011.

M.C. Wheeler and H.H. Hendon. An All-Season Real-Time Multivariate MJO Index : Development of an Index for Monitoring and Prediction. *Monthly Weather Review*, 132 :1917–1932, 2004.

G-Y. Yang and J. Slingo. The Diurnal Cycle in the Tropics. *Monthly Weather Review*, 129 :784–800, 2001.

C. Zhang. Madden-Julian Oscillation. *Reviews of Geophysics*, 43, 2005.

H-M. Zhang, R.W. Reynolds, and J.J. Bates. Blended and gridded high-resolution global Sea Surface Wind speed and climatology from multiple satellites : 1987-present. 2006.

List of figures

List of tables